ANNUAL REVIEWS

Annual Review of Fluid Mechanics

Particle-Laden Turbulence: Progress and Perspectives

Luca Brandt[1,2] and Filippo Coletti[3]

[1]FLOW, Department of Engineering Mechanics, KTH Royal Institute of Technology, Stockholm, Sweden; email: luca@mech.kth.se

[2]Department of Energy and Process Engineering, Norwegian University of Science and Technology (NTNU), Trondheim, Norway

[3]Department of Mechanical and Process Engineering, ETH Zurich, Zurich, Switzerland

ANNUAL REVIEWS CONNECT

www.annualreviews.org

- Download figures
- Navigate cited references
- Keyword search
- Explore related articles
- Share via email or social media

Keywords

particle-laden flows, turbulence, two-way coupling, clustering, gravitational settling, finite-size effects

Abstract

This review is motivated by the fast progress in our understanding of the physics of particle-laden turbulence in the last decade, partly due to the tremendous advances of measurement and simulation capabilities. The focus is on spherical particles in homogeneous and canonical wall-bounded flows. The analysis of recent data indicates that conclusions drawn in zero gravity should not be extrapolated outside of this condition, and that the particle response time alone cannot completely define the dynamics of finite-size particles. Several breakthroughs have been reported, mostly separately, on the dynamics and turbulence modifications of small inertial particles in dilute conditions and of large weakly buoyant spheres. Measurements at higher concentrations, simulations fully resolving smaller particles, and theoretical tools accounting for both phases are needed to bridge this gap and allow for the exploration of the fluid dynamics of suspensions, from laminar rheology and granular media to particulate turbulence.

1. INTRODUCTION

Turbulent flows laden with inertial particles (i.e., particles whose response time is not vanishingly small) are ubiquitous in natural and engineering settings. The richness and complexity displayed by these flows is well known: The different particle and fluid/flow properties, the multiway coupling between dispersed and continuous phases, and the enormous disparity of scales, as reflected in the large number of governing parameters, have made such flows a formidable challenge for experimentalists and modelers alike. Driven by the practical relevance of the problem, particle-laden turbulence has attracted renewed attention in the last decade, also thanks to the tremendous advances of our measurement and simulation capabilities. This review is indeed motivated by the fast progress in our understanding since the last review of the topic (Balachandar & Eaton 2010), for which we need to thank the sustained efforts from multiple research groups around the world. The subject matter is vast, and thus we limit our attention to the case of archetypical turbulent flows (homogeneous turbulence and fully developed wall-bounded flows) laden with spherical rigid particles, heavier than or at most with the same density as the incompressible Newtonian fluid. Recent reviews have addressed the behavior of nonspherical (Voth & Soldati 2017) and light particles, as well as bubbles (Mathai et al. 2020, Risso 2018). We begin by presenting the parameter space, as defined by convenient nondimensional numbers, and the dynamical regimes identified therein. We only briefly summarize the modern toolbox used in laboratory observations and numerical simulations (Section 2) and focus on the flow physics. This is discussed by broadly distinguishing between particles small (Section 3) and large (Section 4) with respect to the minimal scales of the flow, as this distinction has marked possibly the most significant advancements in recent years. We highlight areas that appear especially ripe for progress and where, in our opinion, there is need for systematic and synergic efforts.

We consider spherical particles of diameter D_p and density ρ_p in a fluid of density ρ_f and kinematic viscosity $\nu = \mu/\rho_f$. Under the assumptions invoked for Stokes drag (creeping motion in a uniform and steady flow), the particle response time τ_p can be defined in two ways: the characteristic time to follow a step change of the surrounding fluid velocity, $\rho_p D_p^2/(18\mu)$, or the time to reach the terminal settling velocity when released in a quiescent fluid, $(\rho_p - \rho_f)D_p^2/(18\mu)$. The two definitions converge for $\rho_p/\rho_f \gg 1$. Strictly, inertial particles in turbulent flows violate the Stokes drag assumptions, and empirical corrections are often used to account for the finite particle Reynolds number, Re_p, based on some measure of the particle–fluid slip velocity. The fluid turbulence is characterized by a dissipation rate that defines the Kolmogorov scales η, τ_η, and u_η for length, time, and velocity, respectively. In wall-bounded flows, the near-wall dynamics is governed by the viscous scaling, denoted with the superscript $^+$. Among the various nondimensional groups defining the problem, the density ratio ρ_p/ρ_f, the size ratio D_p/l_f, and the Stokes number $St \equiv \tau_p/\tau_f$ appear as natural choices, where l_f and τ_f are respectively appropriate length and timescales of the flow. Unless otherwise stated, we take the latter to be the Kolmogorov scales, due to the significance of the particle interaction with the microscale structure of the turbulence. Thus, under Stokes drag assumptions, we write $St = 1/18(\rho_p/\rho_f)(D_p/\eta)^2$ and define the settling velocity parameter $Sv \equiv \tau_p g/u_\eta$, where $\tau_p g$ is the terminal velocity in a quiescent fluid under the gravitational acceleration g. The importance of the latter compared to the fluid acceleration is quantified by the Froude number $Fr \equiv a_\eta/g = St/Sv$, where $a_\eta = u_\eta/\tau_\eta$ is the Kolmogorov acceleration. For large particles the fall speed is not known a priori, and the problem is defined by the ratio of a gravitational velocity scale $u_g \equiv [(\rho_p/\rho_f - 1)D_p g]^{1/2}$ and the viscous velocity, used to form the Galileo number $Ga \equiv u_g D_p/\nu$ (alternatively the Archimedes number $Ar = Ga^2$), relating buoyancy and viscous effects. Considering suspensions of large numbers of particles, their concentration becomes important. This is often expressed as the volume fraction Φ_V, i.e., the fractional
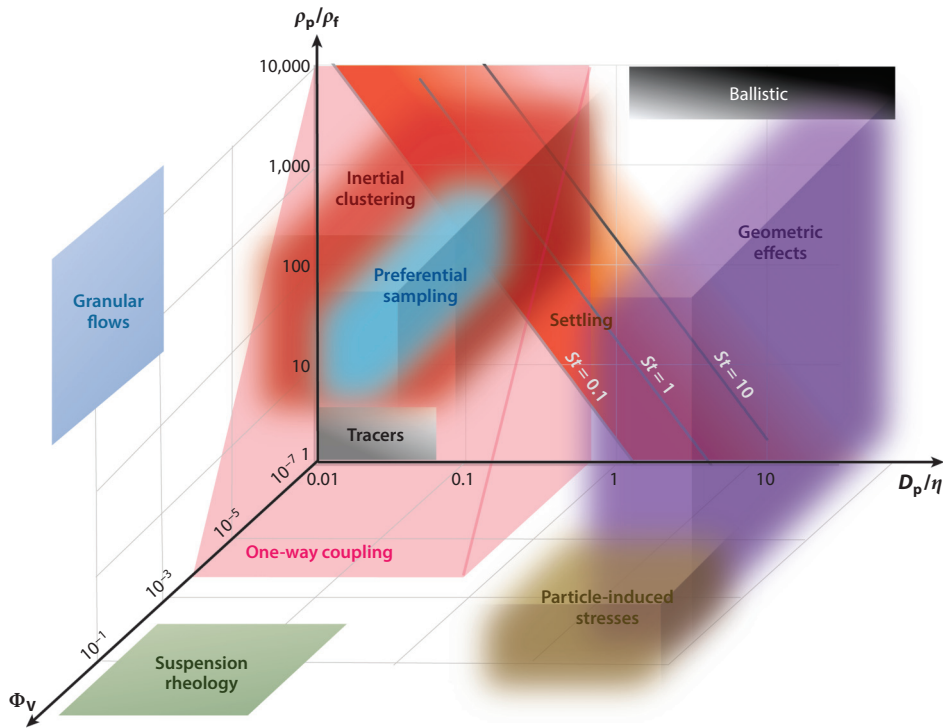
Figure 1

Three-dimensional view of the different regimes characterizing the transport of spherical particles in turbulence. The phase space is defined by the particle size compared to the smallest turbulence scales D_p/η, the particle-to-fluid density ratio ρ_p/ρ_f, and the solid-phase volume fraction Φ_V. For clarity, some regimes are confined to the planes associated with the two variables most essential to their definition.

volume occupied by the particles in the two-phase system, or the mass fraction $\Phi_M \equiv \rho_p \Phi_V / [\rho_p \Phi_V + \rho_f (1 - \Phi_V)]$. For $\Phi_V \ll \rho_f / \rho_p \ll 1$, we have $\Phi_M \sim \Phi_V \rho_p / \rho_f$.

Figure 1 presents a simplified and approximate regime diagram in the parameter space defined by D_p/η, ρ_p/ρ_f, and Φ_V. To limit clutter, we confine some regimes to the planes associated with the two variables most essential to their definition, although the influence of the third variable may not be negligible. Other independent parameters, such as the Reynolds number of the turbulence, Re, enter indirectly through the definition of η. Because typically we have $Fr = \mathcal{O}(10^{-1})$ for industrial and natural turbulent flows, gravitational settling is important above $St = \mathcal{O}(10^{-1})$ and, hence, above $Sv = \mathcal{O}(1)$. In order for the particles not to affect the turbulence (one-way coupling), the volume and mass fraction need to be small (Balachandar & Eaton 2010), and the particle size should be smaller than the Kolmogorov scales.

As shown in **Figure 1**, preferential sampling and inertial clustering characterize the dynamics of dilute and small heavy particles in turbulence, with $St = \mathcal{O}(10^{-1}-10)$. Increasing the number of particles, we move outside the one-way coupling regime and one needs to consider the effect of the suspended phase on the flow. As particles become larger than the smallest flow structures (so-called finite-size particles), geometric effects associated with the local deformation of the fluid flow become important. These particle-induced stresses increase with increasing concentrations. Due to the limitations in our ability to measure and simulate intermediate regimes, the community has studied almost separately small heavy particles in dilute conditions and, more

recently, dense suspensions of large and almost neutrally buoyant particles. The space we consider in this review is complementary to granular flows characterized by high concentrations of massive particles (Forterre & Pouliquen 2008) and viscous suspensions that are better described by the mixture rheology than by the dynamics of discrete particles (Guazzelli & Morris 2012).

2. MODERN METHODOLOGIES

2.1. Experimental Approaches

The vast majority of current experimental studies employ imaging techniques measuring the particle motion via either particle image velocimetry (PIV) or particle tracking velocimetry (PTV), which return Eulerian and Lagrangian information of the particle field, respectively (Adrian et al. 2011). These techniques, however, were developed for single-phase flows where the particles act as tracers, faithfully following the flow; adapting them to inertial particles requires precautions. PIV relies on the assumption that all particles in each interrogation window (which effectively sets the spatial resolution of the measurement) move with the same velocity. This clashes with the significant uncorrelated component of the velocity of nearby inertial particles (see Section 3.1.2); thus, PIV fields should rather be interpreted as a measure of the correlated motion (Carter et al. 2020). PTV algorithms, in contrast, aim at tracking individual particles across successive images, often relying on a predictor–corrector scheme that minimizes the acceleration along the Lagrangian trajectories (Ouellette et al. 2006). Such a strategy may fail when inertial particles collide and rebound with each other or against a wall, but alternative approaches have not been codified yet.

The attention to the spatial distribution and motion of individual particles has resulted in the prevalence of PTV over PIV studies, often time resolved (Lagrangian particle tracking). A specific challenge is related to the particle image: This can be very different from standard tracers, for which subpixel accuracy is attainable by three-point Gaussian fitting. Large and reflective particles can appear as blobs of several saturated pixels. Petersen et al. (2019) showed that their centroid can still be located with ∼0.1 pixel accuracy by a least-squares Gaussian fit. However, the accurate reconstruction of velocities and accelerations requires even higher precision in the particle position, and smoothing is needed to limit noise amplification by differentiation. A common strategy to obtain velocity and acceleration is to convolve the particle positions with the first and second derivative of a Gaussian kernel. This approach was demonstrated for tracers by Voth et al. (2002) and later used in several studies of inertial particle dynamics (e.g., Gibert et al. 2010, 2012).

In order to fully characterize the two-phase flow, one can use simultaneous PIV and PTV on the continuous and dispersed phase, respectively. This requires distinguishing between tracers and inertial particles, typically based on their image size and intensity (Khalitov & Longmire 2002) and digital/optical filtering (Kiger & Pan 2000). The availability of larger and more sensitive camera sensors and higher data rates has supported the adoption of this approach (van Hout 2013). The cross-interrogation of PTV and PIV fields can also be leveraged by using, for example, the PIV fluid velocity as a predictor in the PTV algorithm (Baker & Coletti 2021).

Multicamera volumetric imaging (or single-camera via holographic techniques) allows one to address questions that require 3D reconstruction of the particle trajectories. While 3D tracking was traditionally limited to very low number densities due to ambiguities in the stereoscopic reconstruction, the Shake-The-Box algorithm (Schanz et al. 2016) has greatly alleviated this constraint. Taking advantage of temporally resolved data, this method optimizes the particle matching between successive images by "shaking" the particles around their predicted position and searching for improvements on the projection. For single-phase flows, it has been shown to handle tracer concentrations orders of magnitude higher than those handled by classic algorithms (Discetti &

Coletti 2018). The very few applications to inertial particles to date indicate a remarkable performance (Ebrahimian et al. 2019).

2.2. Numerical Approaches

The most noticeable advance in recent years has been the rapid diffusion of numerical methods for interface-resolved or particle-resolved direct numerical simulations (PR-DNS). These have been recently thoroughly reviewed by Maxey (2017). In addition, we mention here body-fitted methods, in particular, recent overset-grid approaches (Koblitz et al. 2017, Vreman 2017, Horne & Mahesh 2019). These methods use two grids: a body-fitted structured orthogonal grid for the particle, overset on a background grid and on grids associated to other particles. Interpolation schemes are used to match numerical solutions of the two overlapping grids. These methods are ideal for dilute systems and for highly inertial particles (high Re_p) when the cost of handling two grids is compensated by the flexibility of an irregular mesh with local refinement around each particle. Cut-cell methods [for the case of rigid particles, see Schneiders et al. (2013, 2016)] are also gaining favor, as they cure numerical discontinuities due to the particle motion over an underlying fixed grid and allow for a lower resolution than traditional immersed-boundary methods.

Although the combination of efficient algorithms and large-scale supercomputers has enabled the simulations of hundreds of thousands particles in turbulent flows, the availability of huge data sets is not paired by a corresponding improvement of postprocessing tools. We see the need for theoretical efforts to guide the extraction of relevant quantities from the simulation data, e.g., mesoscale stresses and interphase energy fluxes, which would also need to take into account the specific numerical algorithm. We also note, in agreement with remarks by Maxey (2017), that an accurate modelling of lubrication and contact forces, short-range interaction forces, and granular friction is crucial in many configurations and will open new opportunities. To this end, collaborations with experimentalists will be fundamental.

In the case of particles smaller than the smallest flow scales, traditional point-particle direct numerical simulations (PP-DNS) are still the method of choice despite their well-known shortcomings. In particular, the difficult definition of a reference velocity far from the particle and the subtleties of imposing a localized source/sink of momentum in the discretized Navier–Stokes equations make it difficult to accurately simulate even the simple case of settling in a quiescent fluid (see, among others, Kuerten 2016). These have motivated the search for more accurate algorithms by Capecelatro & Desjardins (2013), Gualtieri et al. (2015), Horwitz & Mani (2016, 2018), Akiki et al. (2017), Esmaily & Horwitz (2018), Battista et al. (2019), Horwitz et al. (2020), and Pakseresht et al. (2020). Results obtained with these improved models are reviewed below.

3. SMALL PARTICLES

3.1. Homogeneous Turbulence

Besides being a canonical case in the literature, homogeneous turbulence presents a major advantage for assessing the fluid–particle interaction: the ratio between the particle scales and the flow scales is independent of the spatial location. Indeed, most of the hallmark features of particle-laden turbulence have been demonstrated in such a setting.

3.1.1. Spatial distribution of small inertial particles. Large space-time fluctuations of the local particle concentration appear for a wide range of the parameter space, a phenomenon known as inertial clustering. This has been documented in numerous laboratory experiments and numerical simulations, and recently even by field measurements in atmospheric flows (**Figure 2**). It is
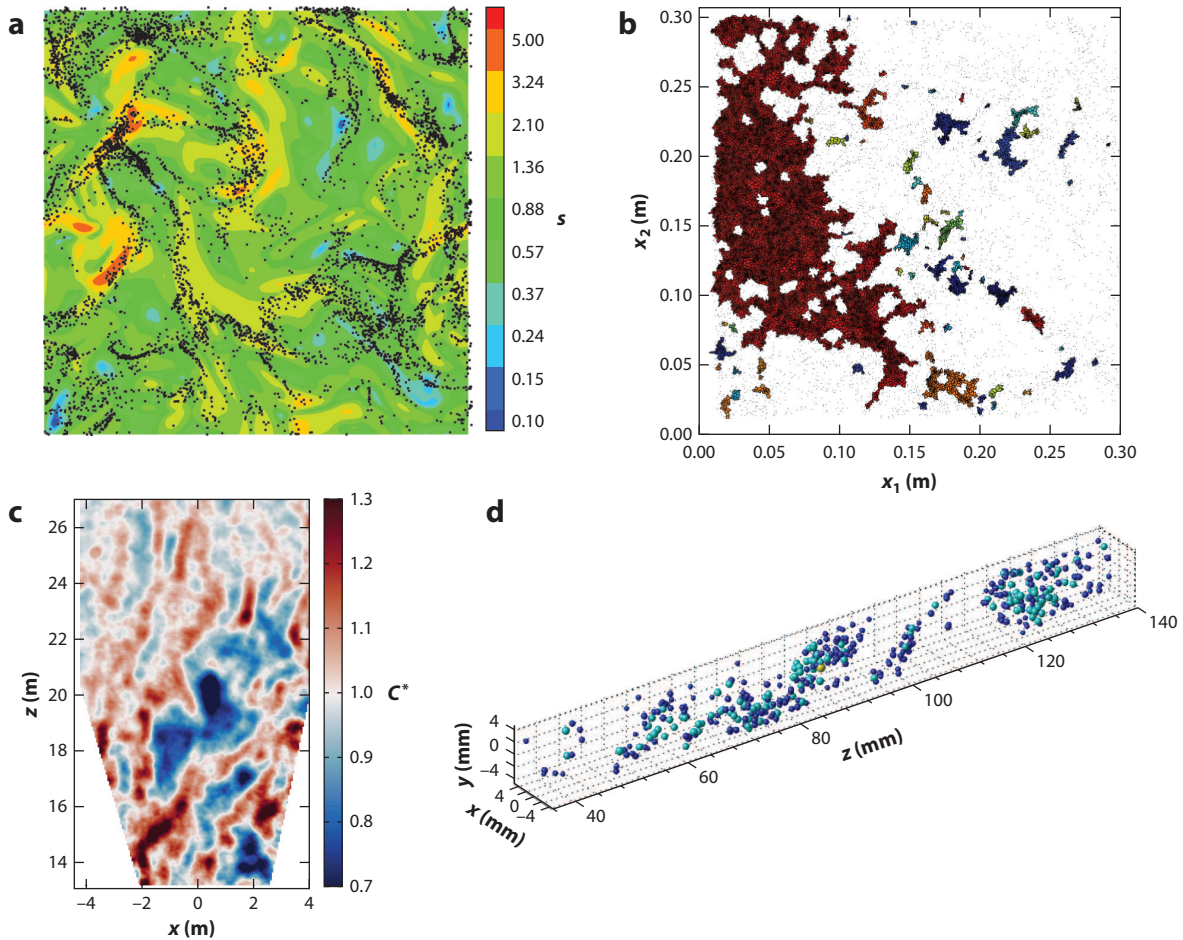
Figure 2

Examples of inertial clustering. (*a*) Particles accumulating in regions of high strain rate (indicated by the colorbar and normalized by the mean value) from point-particle direct numerical simulations of homogeneous isotropic turbulence laden with particles with a Stokes number of $St = 1$. (*b*) Individual clusters (each in a different color) identified by a Voronoi tessellation from laser imaging of homogeneous turbulence laden with $St = 4.6$ particles. Panel *b* adapted with permission from Petersen et al. (2019). (*c*) Relative concentration of snow particles (mean diameter of 0.4 mm) in atmospheric turbulence illuminated by a vertical light sheet (z indicates the height from the ground). (*d*) Three-dimensional spatial distribution of cloud droplets smaller (*blue*) and larger (*cyan*) than 10 μm, measured in situ by an airborne digital in-line holography system. Panel *d* adapted with permission from Beals et al. (2015).

distinct from the clustering observed in dense granular media, which is intrinsic to the solid phase (Fullmer & Hrenya 2017), and it results instead from the combination of the dispersed phase inertia and the fluid turbulence. The mechanism has traditionally been associated with the tendency of inertial particles to visit flow regions of a specific topology, often termed preferential sampling. Numerous numerical studies have confirmed that particles are less likely to be found in regions of high vorticity than in those of high strain, supporting the view that they are centrifuged out of vortex cores. It was later questioned whether such a centrifuge mechanism is the only (or even the main) cause of clustering. Before discussing its origin, we review the principal approaches to quantify clustering and preferential sampling, along with the main findings these have brought to light.

3.1.1.1. Inertial clustering.

As the distribution of particles in turbulence is affected by and is realized over a multitude of scales, the full characterization of clustering is not straightforward, and a variety of methods have been used (Monchaux et al. 2012). Early works (Fessler et al. 1994, Aliseda et al. 2002) leveraged the box-counting method and confirmed the numerical observation of Wang & Maxey (1993) that clustering is most pronounced for $St = \mathcal{O}(1)$. Studies using radial distribution functions (RDFs) could achieve a scale-by-scale quantification of clustering and confirmed its typical length scale to be $\mathcal{O}(10\eta)$ (Saw et al. 2008). Gualtieri et al. (2009) employed the angular distribution function (ADF) to consider the orientation of the separation vector between particles and showed that clustering in sheared turbulence is anisotropic down to the dissipative scales. For $St < 1$ and separations within the dissipative range, experiments (Saw et al. 2008, Petersen et al. 2019) and simulations (e.g., Ireland et al. 2016a) found a power law behavior of the RDF—a hallmark of geometric self-similarity. At higher St, particles are weakly responsive to the small-scale eddies and cluster at inertial-range scales, over which the distribution is no longer scale invariant (Bec et al. 2007) and the RDFs decay exponentially (Petersen et al. 2019). At sub-Kolmogorov separations comparable with the particle diameter, Yavuz et al. (2018) found that the RDF deviated from the power law scaling and reached higher levels, which they attributed to interparticle hydrodynamic interactions. The implications may be profound since the RDF value at the particle radius is at the core of collision models (Pumir & Wilkinson 2016).

Various authors have investigated the Lyapunov exponents of inertial particle trajectories, i.e., their rate of exponential separation/approach, in synthetic flows (Wilkinson & Mehlig 2005, Ijzermans et al. 2010) and PP-DNS (Bec et al. 2007). This analysis is only applicable over the dissipative scales where the fluid flow is smooth. It was shown that clustering occurs over multifractal sets in the phase space spanned by the particle positions and velocities. Additionally, particles can theoretically accumulate in singular regions of unbound concentration and filamental shape called caustics, where the particle velocity field becomes multivalued (Wilkinson & Mehlig 2005).

Monchaux et al. (2010) introduced the use of Voronoi diagrams to characterize inertial clustering: The domain is divided into cells attached to each particle, the inverse of the cell volume defining the local concentration. For particles randomly located in space, the PDF (probability density function) of the cell sizes is well approximated by a Γ distribution (Ferenc & Néda 2007), while inertial particles show a broader PDF. Individual clusters can be defined as sets of particles contained in connected groups of cells smaller than a given threshold. Above a certain size, the clusters possess convoluted shapes associated with a distinct fractal dimension and follow a power law size distribution that stretches to the integral scales (Sumbekova et al. 2017, Petersen et al. 2019). Such features have also been recognized in field imaging of snow particles falling in turbulent air (Li et al. 2021). The mean cluster size tends to grow with St and Re, and the in-cluster concentration is about one order of magnitude larger than the mean, irrespective of the cluster size (Baker et al. 2017). Liu et al. (2020) used the Voronoi method to track inertial particles ($St > 1$) before, during, and after the cluster lifetime. They found that the latter typically lasts a few Kolmogorov timescales, increasing with the cluster size; small clusters usually coagulate from and disintegrate into nonclustered particles, while large clusters recombine into other large clusters.

While versatile, the Voronoi method is prone to subsampling bias: If the particle number density is low, important observables are affected, including the standard deviation of the Voronoi cell size distribution (Monchaux 2012) and the fraction of clustered particles compared to the total (Momenifar & Bragg 2020).

3.1.1.2. Preferential sampling.

The tendency of inertial particles to favor distinct flow features is often assessed by measuring the correlation between particle position and local fluid observables, the most scrutinized being the strain rate and its prevalence relative to enstrophy. Various metrics

were reported: the concentration conditioned on the level of strain rate or enstrophy (Petersen et al. 2019), PDFs of the Q-criterion (Hunt et al. 1988) at the particle location (Baker et al. 2017), and joint PDFs of concentration and enstrophy (Frankel et al. 2016). The evidence is that, for $St = \mathcal{O}(1)$ and below, the particles oversample regions where strain overwhelms rotation, consistently with the centrifuge mechanism. This tendency, however, is weak or absent for more inertial particles (Coleman & Vassilicos 2009) or in presence of significant gravity effects (Frankel et al. 2016).

Preferential sampling of high-strain/low-enstrophy regions has rarely been documented in fully turbulent flow experiments. Gibert et al. (2012) measured the mixed particle velocity–acceleration structure function in a von Karman flow and showed trends consistent with preferential sampling of high-strain regions. Petersen et al. (2019) found that only a slight majority of the particles were in strain-dominated regions in the range $St = 0.37$–5.4.

3.1.1.3. Clustering mechanisms.

The argument behind the centrifuge mechanism is strictly applicable only in the regime $St \ll 1$, for which the compressibility of the particle velocity field is directly related to the excess of strain over rotation (Maxey 1987). However, clustering is most intense for $St = \mathcal{O}(1)$. Finite-St particles lag the flow and therefore their spatial distribution cannot be fully determined by the instantaneous fluid velocity field. Moreover, clusters are multiscale in nature, stretching above and below the dimension of the Kolmogorov-size vortices. Additionally, clustering is also manifest in random flows that lack any topological structure (Bec 2003).

These considerations have triggered intense efforts to understand inertial clustering beyond the centrifuge mechanism. Bec (2003) and Bec et al. (2006) used random flows and PP-DNS to show that, for increasing St, the dominant factor becomes the lagging of the particles. Infinitesimal clouds of particles shrink over time and lead to clustering over fractal sets; while particle blobs in the inertial range contract at a rate dependent on the scaling properties of the pressure field (Bec et al. 2007). Bragg & Collins (2014) also argued that the centrifuge mechanism is only dominant for $St \ll 1$, while outside this regime it gives way to a path-history mechanism: The particle dynamics decouples from the local fluid velocity field and past interactions with turbulent events become increasingly important. Statistical mechanics calculations have showed that small-scale clustering is driven by a multiplicative amplification process of random contractions and expansions (Gustavsson & Mehlig 2016). In the small-St limit, the particles are driven by the instantaneous flow, while in the opposite limit they uniformly sample the turbulence and cluster due to history effects. The importance of the latter was also highlighted by Liu et al. (2020), who showed that, for $St \gtrsim 1$, clusters form during a phase in which the small-scale turbulence activity (tracked along the particle trajectories) decays, and they survive as long as such a quiet state persists. The sweep-stick mechanism (Chen et al. 2006) is instead based on the view that zero-acceleration points in the flow are swept by the large-scale eddies, and particles stick to those because they move (to first order) at the same velocity. Coleman & Vassilicos (2009) argued that the mechanism would hold also for τ_p in the inertial range, supplanting the centrifuge mechanism at intermediate to large scales, where clustering results from larger eddies sweeping smaller ones, irrespective of St.

Many simulations do not include the effect of gravity. The assumption of $Fr \gg 1$, however, is only meaningful under dissipation levels rarely achieved in terrestrial environments: in the atmosphere and in the ocean, we typically have $Fr \ll 1$ (Shaw 2003, Ivey et al. 2008). Several simulations have noted that heavy particles falling in homogeneous turbulence form vertically elongated clusters (Bec et al. 2014), as confirmed by experiments (Petersen et al. 2019). This anisotropy was quantified by ADFs (Ireland et al. 2016b) and by the orientation of the primary cluster axis (Baker et al. 2017). Because these simulations assumed one-way coupling, anisotropy cannot be

rooted in multiparticle hydrodynamic interactions. The proposed explanations have included a two-dimensionalization of the dynamics in the horizontal plane (Bec et al. 2014) and the channeling of particles by downward turbulent gusts (Baker et al. 2017).

3.1.2. Motion of inertial particles.
The spatial distribution of the particles is of course the result of their motion in the turbulent fluid. Even in the simplest case of a one-way coupled regime, the problem is highly complex.

3.1.2.1. Maxey–Riley–Gatignol equation.
The heart of the point-particle approach is the Maxey–Riley–Gatignol (MRG) equation of motion (Maxey & Riley 1983, Gatignol 1983), which describes the forces acting on a small particle in arbitrary motion in an unsteady nonhomogeneous flow. Its rigorous derivation requires vanishing Re_p, so that different forces can be linearly superposed, and extremely dilute concentrations, so that interparticle effects can be ignored. The equation has frequently been used outside of these assumptions, calling for a thorough assessment of the limits of the framework. For small heavy particles, scaling arguments show that gravity and drag are dominant (Ling et al. 2013). The drag force is often modelled by correcting the Stokes formula for finite Re_p (e.g., Schiller & Naumann 1933). While such corrections were derived in homogeneous and steady conditions, comparisons against experiments and PR-DNS showed good performance in simple cellular configurations (Bergougnoux et al. 2014) and low-Re turbulence, $Re_p = \mathcal{O}(1)$ (Mehrabadi et al. 2018). In high-Re turbulence, however, the probability of extreme events was underestimated (Saw et al. 2014). Ling et al. (2013) showed that, even for $\rho_p/\rho_f \gg 1$, unsteady forces in the MRG equation (added mass, fluid acceleration, and history force) become significant as soon as D_p is comparable to η. The relevance of the history term, often neglected partly due to its high computational cost, has been recently rediscovered: Its importance for particle kinematics (Daitche & Tél 2011) and clustering (Olivieri et al. 2014) has been highlighted, and efficient approaches for its calculation have emerged (Prasath et al. 2019).

The scrutiny of the MRG equation has not been limited to its individual terms, extending to its dynamical system behavior. Sapsis et al. (2011) showed in a 2D chaotic flow that the deterministic nature of MRG did not capture random correlated fluctuations of inertial particle velocities and proposed stochastic model corrections. Haller & Sapsis (2008) derived a reduced-order equation governing the asymptotic motion of particles on a slow manifold, which arises for small St. Wan & Sapsis (2018) utilized this slow-manifold reduction as a first-order model of the particle motion and employed a machine learning strategy with recurrent neural networks (trained by the full MRG equation for particles in a simple cellular flow) to obtain the higher-order terms.

3.1.2.2. Fluctuating energy, acceleration, and dispersion.
For nonballistic particles, the fluctuating energy per unit mass of the dispersed phase k_p is comparable to the fluid turbulent kinetic energy k_f (Good et al. 2014, Ireland et al. 2016a). For $St < 1$, k_p can exceed k_f because of preferential sampling of energetic fluid regions; while for $St > 1$ the dynamics is dominated by inertial filtering, i.e., the inability of the particles to respond to fast fluid fluctuations—hence, $k_p < k_f$. Due to history effects, the fluctuating velocity of heavy particles possesses an uncorrelated component, increasingly prominent for larger St (Février et al. 2005, Wilkinson & Mehlig 2005). Inertial filtering also limits particle acceleration (Toschi & Bodenschatz 2009) and slows down the decay of the particle velocity autocorrelation, in turn enhancing single-particle dispersion compared to tracers (Sabban & van Hout 2011). Inertia also enhances two-particle dispersion at small times due to the uncorrelated motion at small separations (Bec et al. 2010, Gibert et al. 2010), while for longer times, inertial filtering and path-history effects reduce pair dispersion compared to tracers (Bragg et al. 2016).

The effect of gravitational drift (or trajectory-crossing) has been recognized since Yudine (1959), yet only recently has the full impact of gravity on the particle motion been systematically investigated. Good et al. (2014) showed that k_p/k_f decreases with Sv, in agreement with the analytical model by Wang & Stock (1993). Simulations (Ireland et al. 2016b) and experiments (Berk & Coletti 2021) have showed that, as the temporal derivative of the sampled-fluid velocity is augmented by gravitational drift, so is the particle acceleration. Inspired by Csanady (1963), Berk & Coletti (2021) proposed analytical models for the particle velocity and acceleration variances. These are based on the Lagrangian energy spectrum of the particle velocity, obtained from the spectrum of the fluid sampled by the particles and modulated by their response time. The effect of gravity is incorporated through a simple model of the sampled-fluid timescale. **Figure 3** illustrates how the model compares with experimental and numerical data and captures the complex dependence on St and Fr—in particular, how gravity hinders velocity variance while augmenting acceleration variance.
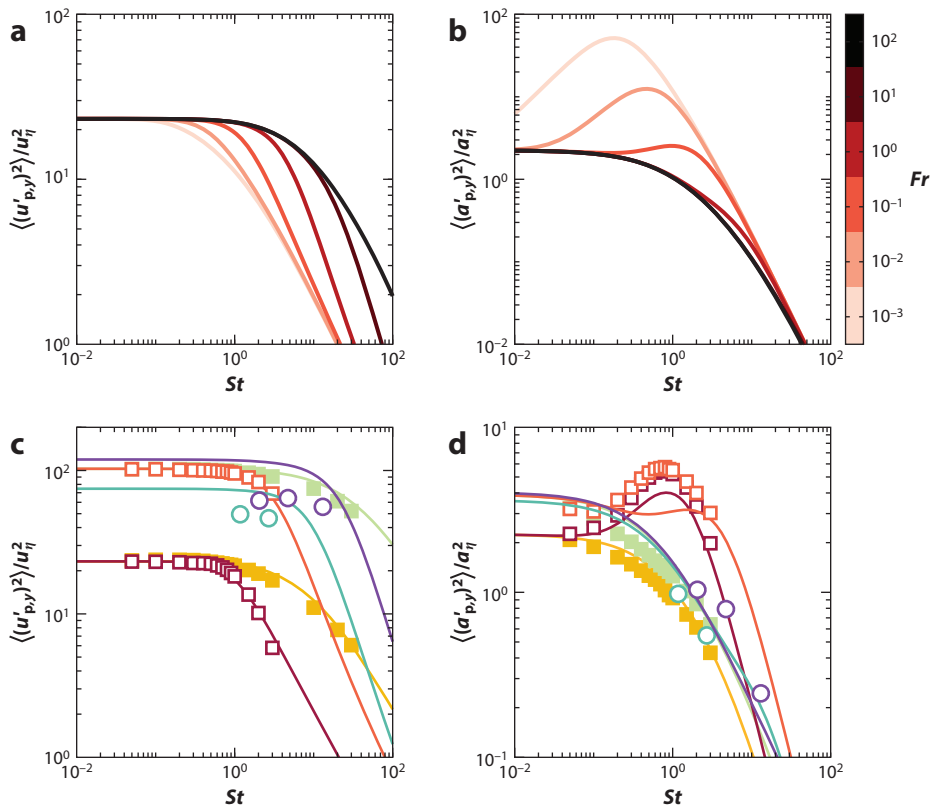

Figure 3

Variance of the particle vertical (*a*) velocity, $\langle (u'_{p,y})^2 \rangle / u_\eta^2$, and (*b*) acceleration, $\langle (a'_{p,y})^2 \rangle / a_\eta^2$, in Kolmogorov scaling, as a function of the Stokes number St and Froude number Fr for Taylor Reynolds number $Re = 300$, as predicted by the analytical model of Berk & Coletti (2021). The predictions are compared with (*c*) velocities and (*d*) accelerations from measurements [*open circles* (Berk & Coletti 2021)] and point-particle direct numerical simulations [*open squares* (Ireland 2015; Ireland et al. 2016a,b)]. Filled squares are for zero-gravity simulations.

3.1.2.3. Gravitational settling.

While several mechanisms have been theorized by which turbulence can either enhance or hinder settling (Good et al. 2012), for small dilute particles in homogeneous shearless turbulence, most studies have reported settling enhancement. This is often explained by preferential sweeping, i.e., the oversampling of downward regions of the turbulent eddies (Maxey 1987, Wang & Maxey 1993, Petersen et al. 2019). The mechanism was invoked by Nemes et al. (2017) and Li et al. (2021) to explain field observations of snow fall speed. The inverse argument was used to explain the reduced rising velocity of bubbles in turbulent water, as these are expected to oversample vortex cores (Aliseda & Lasheras 2011). Interestingly, particles only slightly lighter than the fluid are actually driven out of vortex cores by the added mass force, leading to an upward preferential sweeping that increases the rising velocity (Ruiz et al. 2004, Marchioli et al. 2007). Although the pictorial representation of this mechanism is similar to the centrifuging by vortex cores, the particle concentration correlates much more markedly with downward fluid fluctuations than with high-strain regions (Petersen et al. 2019). Both St and Sv shall be of order unity to warrant a significant settling enhancement (Good et al. 2014), but it is still debated which velocity scale governs it. While various studies have indicated that settling enhancement is proportional to the root-mean-square of the fluid velocity fluctuations (e.g., Huck et al. 2018), Tom & Bragg (2019) showed by theory and simulations that preferential sweeping is driven by a range of velocity scales whose width increases with St. The actual extent of the settling enhancement has remained an open question until recently. Early experiments from different groups showed large differences, complicating the validation of numerical simulations (Bosse et al. 2006). The quantification of the fall speed of microscopic particles is indeed a difficult task. In wind tunnels the settling rate can be orders of magnitude smaller than the flow speed, while tanks stirred by oscillating grids often generate circulations likely to alter the particle fallout. Chambers stirred by randomly actuated jets can instead create intense turbulence with negligible mean flow and shear. Using this type of facility, Good et al. (2014) and Petersen et al. (2019) obtained similarly large maximum settling velocities, exceeding $2.5\tau_p g$ in very dilute regimes. Such a massive settling enhancement may have major consequences for the transport of particles in natural and industrial settings. This is substantially higher than the predictions from PP-DNS at matching conditions (Good et al. 2014) and is an example of the limits of the point-particle approach even in nominally one-way coupled flows.

3.1.3. Two-way coupling.

One of the most elusive aspects of the problem is the back-reaction of inertial particles on the fluid, termed two-way coupling. The regime map by Elghobashi (1994) is often referenced to claim one-way or two-way coupling when Φ_V is smaller or larger than 10^{-6}. This classification has been shown to hold approximately true for gas–solid systems (Petersen et al. 2019) but not for solid–liquid systems, where typically no evidence of turbulence modification is found below $\Phi_V \sim 10^{-4}$ (Poelma et al. 2007, Baker & Coletti 2021). It remains controversial whether the turbulence is augmented or attenuated, and to which extent. This is partly due to multiple competing mechanisms (Balachandar & Eaton 2010), and systematic studies are needed where one parameter at a time is varied. Numerical efforts are most suited for this purpose, but turbulence modification has proven to be extremely challenging to model correctly. We touch upon some of the most notable aspects.

In standard two-way-coupled PP-DNS, the drag force is projected back to the fluid grid. This is problematic when the particles are not much smaller than the grid spacing, and when they are so dilute to produce a nonsmooth force field (Eaton 2009). Capecelatro & Desjardins (2013) proposed a regularization procedure in which the projection is performed using a compact Gaussian stencil, which is diffused to the surrounding points even if the particle size is comparable to the

grid spacing. Importantly, the particle–fluid slip velocity in the drag formulation is based on the undisturbed fluid velocity in the absence of the particle. Such nominal slip velocity is bound to be higher than the actual slip velocity, because of the self-induced disturbance (i.e., the particle dragging fluid with it). This becomes crucial in particle-laden turbulence at significant concentrations, where the undisturbed state is not available. To reconstruct it, recent approaches used analytical solutions to a regularized point-force applied by the particle (Gualtieri et al. 2015, Horwitz & Mani 2016, Ireland & Desjardins 2017, Balachandar et al. 2019). Systematic comparisons with experiments and PR-DNS are needed to verify that these techniques correctly capture turbulence modification.

Another fundamental difficulty concerns the steady simulation of homogeneous particle-laden turbulence, as hydrodynamic forcing leads to interscale energy transfers not easily discernible from the actual interphase coupling (Lucci et al. 2010). Simulations of decaying turbulence are not affected by these issues; however, they quickly drop to weak levels of turbulence intensity, may depend on the initial condition for the dispersed phase, and can be compared only qualitatively against steady measurements.

Experimental studies focused on the modification of homogeneous turbulence remain scarce, as it is difficult to accurately characterize the underlying flow when the volume fraction is significant: For a fixed Φ_V, the number density varies as D_p^{-3}, and separating fluid tracers from small inertial particles via imaging becomes arduous. As such, most previous studies have considered relatively large, quasi-ballistic particles, finding turbulence attenuation (Tanaka & Eaton 2010). Recently, R. Hassaini & F. Coletti (manuscript in preparation) carried out systematic PIV/PTV measurements of particles with $St = \mathcal{O}(1)$ and $Sv = \mathcal{O}(1)$ in homogeneous turbulence, varying Φ_V between 10^{-6} and 5×10^{-5}. They observed the so-called pivoting effect [the enhancement/reduction of turbulence activity at the small/large scales (Poelma & Ooms 2006)] and a monotonic increase of the kinetic energy k_f with particle loading (**Figure 4**). This contrasts with the common view that sub-Kolmogorov particles attenuate turbulence, but it is consistent with the only previous experimental study in a similar regime (Yang & Shy 2005). Two-way coupled PP-DNS also found turbulence enhancement when gravity was considered (Frankel et al. 2016, Rosa et al. 2020), as opposed to the turbulence attenuation in zero gravity (Poelma & Ooms 2006,
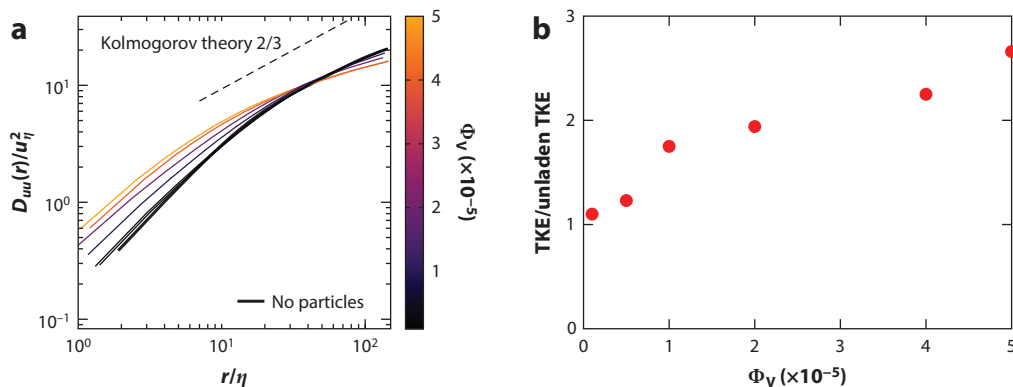

Figure 4

(*a*) Second-order velocity structure function (D_{uu}) as a function of the separation (*r*), both normalized by Kolmogorov scaling, and (*b*) turbulent kinetic energy (TKE) measured by R. Hassaini & F. Coletti (manuscript in preparation) in homogeneous turbulence laden with particles with a Stokes number $St = 2.3$ and settling velocity parameter $Sv = 3.1$ for a range of volume fractions, from $\Phi_V = 10^{-6}$ to 5×10^{-5}.

Saito et al. 2019). Taken together, these results indicate that the net change in $k_{\rm f}$ follows from the competing effect of gravity and drag: Falling particles transfer their potential energy to the flow and do so more effectively at $St = \mathcal{O}(1)$ via the collective action of clusters; while they also act as sinks of fluid momentum by dragging fluid and distorting the flow around them, especially when they behave ballistically.

As the particle loading increases, the source of the fluid fluctuating energy shifts from the hydrodynamic forcing to the relative motion between carrier and dispersed phases. Capecelatro et al. (2015) investigated homogeneous systems in which heavy particles fall at large loadings ($\Phi_V \approx 0.01$, $\Phi_M \approx 10$). The flow is purely gravity driven, with random initial fluctuations growing and giving rise to dense fast-falling clusters. These in turn entrain fluid and sustain large fluctuations, termed cluster-induced turbulence, which is fundamentally different from situations where turbulence drives the particle motion. Turbulence can also be generated in systems in which particles are sources of heat, e.g., when they absorb radiative flux and release it to a transparent carrier fluid, increasing its local temperature. Zamansky et al. (2014, 2016) investigated this case over a large range of $\tau_{\rm p}$, heat flux, and gravitational strength. For sufficient particle inertia, clusters are formed and generate buoyant plumes. Frankel et al. (2016) considered the interplay between buoyant plumes shed by heated heavy particles and hydrodynamically forced turbulence, reporting reduced settling velocity compared to the unheated case. Banko et al. (2020) studied a duct air flow laden with polydisperse nickel particles (mean $St \approx 11$) exposed to near-infrared radiation. They measured large fluid temperature fluctuations comparable to the overall temperature rise, signaling the local radiation absorption by clusters.

3.2. Wall-Bounded Turbulence

The presence of a rigid boundary introduces mean velocity gradients, variations in the level of fluctuations with the distance from the wall, and anisotropies in the near-wall velocity field, as well as well-studied flow structures: quasi-streamwise vortices, low-speed streaks, and, at large Reynolds numbers, the so-called very-large-scale motions (Smits et al. 2011). All these features affect the near-wall particle dynamics, as detailed below.

3.2.1. Spatial distribution and kinematics.
A distinctive feature of particle dispersion in wall turbulence is the drift of particles against the mean gradient of turbulence intensity, termed turbophoresis. The net effect of this migration toward the wall is segregation in the buffer layer, most prominent when the particle relaxation time matches the local turbulence timescale, corresponding to $St^+ = 10\text{–}50$ (Marchioli & Soldati 2002, Sardina et al. 2012, Bernardini 2014). In dilute conditions, inertial particles have been experimentally observed to arrange in long near-wall streaks (Niño & Garcia 1996, Fong et al. 2019), and numerical simulations have demonstrated the role of the near-wall coherent structures in determining their motion (Marchioli & Soldati 2002, Nilsen et al. 2013). At steady state, the particles need to oversample fluid motions departing from the wall region to balance the turbophoretic drift (Picciotto et al. 2005). Hence, localization in low-speed streaks is explained by the local prevalence of fluid ejections. Sardina et al. (2012) showed via ADFs that clustering in the turbulent boundary layer features a strong directional orientation and is much more intense compared to isotropic flows. Moreover, despite the fact that the turbophoresis and clustering are usually addressed separately, these authors argued that they represent different aspects of the same process. They also found that the length of particle streaks is of the order of 10^3 inner units, i.e., much longer than the fluid velocity streaks.

Despite the oversampling of low-speed streaks, in the immediate vicinity of the wall the dispersed phase can travel faster than the fluid, as it does not obey the no-slip boundary condition

(Shokri et al. 2017, Fong et al. 2019). Above the viscous sublayer, the particles lag the flow with a mean slip velocity of the order of the friction velocity. This is partly due to the preferential sampling of low-speed fluid regions, and partly due to the finite time needed to adjust to the fluctuations of the local fluid velocity (Berk & Coletti 2020).

Most numerical simulations of particle-laden wall turbulence have neglected gravity. The interplay between turbulent diffusion and wall-normal gravity is in fact central to aeolian and sediment transport, which largely motivates fundamental research on these regimes. Experiments (Gerashchenko et al. 2008) and simulations (Lavezzo et al. 2010, Lee & Lee 2019) have shown the importance of trajectory-crossing as soon as the terminal particle settling velocity is comparable to the friction velocity: The drift across the different strata of the boundary layer results in increased particle acceleration, which may offset the dampening effect of inertia. The wind tunnel experiments of Berk & Coletti (2020) showed no evidence of turbophoresis on the concentration profiles of suspended glass microspheres; their results could rather be explained by a balance between gravitational settling and turbulent diffusion, as in the classic Rouse–Prandtl theory. Comparing to the latter, they found significantly weaker concentration gradients, which they attributed to the fact that the theory does not account for particle inertia.

Thus far, there have been relatively few detailed experiments focused on particle-laden wall turbulence. Capecelatro & Desjardins (2015) successfully simulated via PP-DNS the laboratory channel flow of Benson et al. (2005) laden with quasi-ballistic particles ($St = 90$). Regimes leading to clustering and turbophoresis have proven more challenging. Fong et al. (2019) considered a vertical channel flow with $St \sim 7$ particles and found that, near the wall, the dispersed phase reached substantially lower concentration and higher velocity fluctuations compared to PP-DNS at matching conditions (G. Wang et al. 2019). An underappreciated source of discrepancy might be represented by the modeling of wall–particle and particle–particle collision: In the regime considered by Fong et al. (2019), the restitution coefficient is highly dependent on the impact velocity (Gondret et al. 2002), an effect usually neglected by PP-DNS.

Interface-resolved simulations of relatively small particles, enabled by massive computational resources, are proving useful to pinpoint specific areas of improvement in lower-order models. Costa et al. (2020) considered heavy particles ($\rho_p/\rho_f = 100$) in a channel flow under dilute conditions and no gravity, and compared PP-DNS with drag force alone against PR-DNS of particles with $D_p^+ = 3$. Similarly to G. Wang et al. (2019), their results showed that PP-DNS significantly overestimated turbophoresis and underestimated particle velocity fluctuations near the wall. The addition of a Saffman lift force (usually neglected in the standard implementation of the MRG equation for small particles) was shown to improve the predictions, in terms of both concentration peak and first- and second-order moments of the particle velocity, as it greatly reduced the near-wall particle residence time to match the PR-DNS. These data suggest the need to improve upon existing correlations for particle–fluid forces, particularly in proximity of a solid wall. Attempts in this direction have recently exploited machine learning and data-driven tools (Balachandar et al. 2020).

3.2.2. Modification of wall turbulence and drag.
Several studies used two-way coupled and four-way coupled (i.e., including interparticle collisions) PP-DNS to investigate particle-laden wall turbulence, as reviewed by Kuerten (2016). At sufficient loadings, the particles were found to affect the ejection–sweep cycle, the dynamics of streamwise vortices, and the formation and strength of hairpin eddies (Richter & Sullivan 2014). This significantly modifies the Reynolds stresses: These distribute differently among the various components compared to the single-phase scenario, with a reduction of the total turbulent fluid stress. The modifications to the flow, in turn, alter the particle segregation and velocity statistics. In particular, the turbulence modulation and

interparticle collisions were found to reduce the near-wall concentration (Kuerten & Vreman 2015).

Due to the abovementioned limitations in representing the particle back-reaction in PP-DNS, ground-truth validation of these findings is sorely needed. However, laboratory observations in this specific regime are even more challenging than in homogeneous turbulence because imaging of the fluid flow in the near-wall region of interest is largely impaired by the high local concentration. Recent experimental studies have been scattered and concerned with disparate regimes. Taken together, the different findings do not provide a coherent picture: For example, Li et al. (2012) found near-wall turbulence enhancement already at $\Phi_V = 10^{-7}$ in a horizontal gas–solid flow, while Shokri et al. (2017) found weak turbulence attenuation at $\Phi_V = 10^{-3}$ in a vertical solid–liquid flow. Clearly, systematic efforts covering wide regions of the parameter space are warranted.

An area of great practical interest is the change of the drag properties in internal flows. While small neutrally buoyant particles are classically assumed to produce an effective increase of the suspension viscosity and, thus, to augment drag (Stickel & Powell 2005), for inertial particles the situation is more complex. Early experiments reported drag reduction in gas–solid suspensions in pipes: Rossetti & Pfeffer (1972) seeded a vertical air flow with micrometric glass beads and found significant drag reduction compared the the single-phase flow. More recently, Zhao et al. (2010) also found by PP-DNS that heavy ($\rho_p/\rho_f \sim 1{,}000$) particles reduced drag in a turbulent channel flow in the absence of gravity, as signaled by an increased flow rate for a fixed driving pressure gradient. Recently, Battista et al. (2019) extended the method of Gualtieri et al. (2015) to account for the vorticity generation due to the particles close to solid boundaries. They showed that the drag of turbulent pipe flows is either unaltered or increased by the particles, unlike the finding of Zhao et al. (2010). The extra stress induced by the particles was found to induce a momentum flux toward the wall that ultimately increased the viscous shear stress and, consequently, the drag. In the same spirit, Horwitz et al. (2020) proposed a discrete Green's function approach for two-way coupled PP-DNS, formally not limited to low particle Reynolds numbers. The results confirmed wall treatment as an important issue when studying turbulence modification by particles, with implications for the statistics of particle-laden turbulent channel flow. PR-DNS can shed light on this aspect. Costa et al.'s (2021) results from particle-resolved simulations of small ($D_p = 3^+$) heavy particles in turbulent channel flow revealed that modulations of the underlying turbulence appear already at $\Phi_V \approx 10^{-4}$ ($\Phi_M \approx 10^{-2}$) (see **Figure 5**). In this regime, the near-wall turbulence keeps its main structure and the solid particles follow the near-wall streak dynamics, with sweep and ejection events, creating particle Reynolds stresses similar to those associated to tracers. The fluid statistics are not significantly different, yet drag increases because the addition of inertial particles augments the force needed to drive the flow. Further increasing the mass loading, $\Phi_V = \mathcal{O}(10^{-3})$, the near-wall turbulence is found to be clearly altered: the fluid velocity fluctuations and the fluid Reynolds stresses decrease, while the total drag further increases. The near-wall streaks become wider and the contribution of the turbulent stresses shrinks while the particle stresses, in particular the particle Reynolds stresses, grow and seize a larger share of the total stresses, ultimately augmenting drag.

4. LARGE PARTICLES

4.1. Homogeneous Flows

The study of finite-size particles in homogeneous turbulent flows is usually motivated by natural flows and industrial processes where gravity plays an important role. Therefore, we briefly review below the particle settling behavior in a quiescent fluid. Then, we discuss in particular how particle settling is affected by the background turbulence and how existing turbulence is affected by the
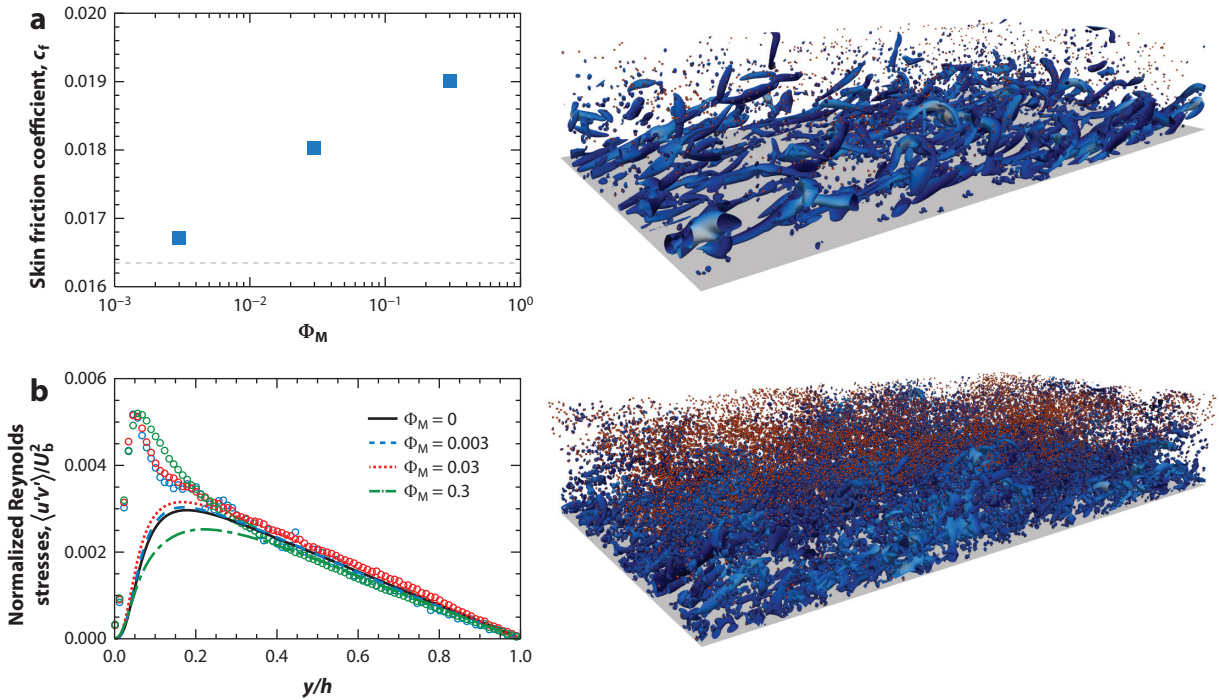
Figure 5

Results of particle-resolved direct numerical simulations of small inertial particles of diameter $D_p^+ = 3$ with density ratio $\rho_p/\rho_f = 100$ in plane channel flow (Costa et al. 2021). (*a, left*) Friction coefficient c_f versus the particle mass fraction Φ_M, showing an increase in drag with the particle concentration. (*b, left*) Wall-normal profiles of the fluid (*solid lines*) and particle (*circles*) Reynolds shear stresses for different Φ_M, revealing a decrease of the fluid stresses at higher concentrations, compensated by increased particle stresses. On the right of each panel are visualizations of particle positions and isosurfaces of the Q-criterion, coloured by the local wall-normal velocity (*blue*, low; *white*, high) for the two largest values of Φ_M: The near-wall turbulent cycle is altered only for $\Phi_M \approx 10^{-2}$.

presence of many particles. The features of the fluctuations generated by particles in a quiescent fluid are also briefly mentioned.

4.1.1. Particle dynamics in an otherwise quiescent fluid.

Starting from the analytical solution in Stokes flow, researchers have moved to consider inertial effects, i.e., the change of speed and drag force at finite particle Reynolds number, and the collective dynamics in suspensions. Studies of large particles in still fluids aim to find the Reynolds number based on the terminal velocity as a function of the Galileo number Ga and ρ_p/ρ_f, the governing independent parameters. Increasing Ga, the particle motion becomes oblique, time periodic, zig-zagging, helical, and chaotic (Jenny et al. 2004, Horowitz & Williamson 2010). Empirical correlations exist and are often used to validate and complement numerical results (Uhlmann & Doychev 2014, Fornari et al. 2016b).

Additional effects come into play when many particles interact with each other. In Stokes flow, the reduction of the mean settling speed in suspensions is explained as a hindrance effect, i.e., the presence of an average upstream fluid motion due to mass conservation (Guazzelli & Morris 2012). At finite inertia, when interactions mediated by the particle wake become important, the settling speed is found to increase due to pair interactions, the so-called drifting–kissing–tumbling (DKT) (Fortes et al. 1987). Fornari et al. (2016b) identified DKT events in suspensions at 0.5% and 1% at $Ga = 145$ that counteracted the hindrance effect. These led to instantaneous settling

speeds twice as large as the mean values, so that without these intermittent events the averaged settling velocity would be smaller by approximately 3%. Below $Ga = 155$, hindrance is dominant in determining the particle settling speed.

As particles shed wakes, they induce fluid velocity fluctuations often termed pseudo-turbulence (Tenneti & Subramaniam 2014). This has been investigated mostly in gas–solid systems at high volume fractions. Mehrabadi et al. (2015) simulated heavy particles at $\Phi_V = 10$–40% and $Re_p = 50$ and showed that the pseudo-turbulent kinetic energy was comparable to that of the fluid motion relative to the particles, and that the induced Reynolds stresses were strongly anisotropic. For lower density ratios, Uhlmann & Doychev (2014) used fully resolved simulations to investigate the settling of dilute suspensions in an otherwise quiescent fluid with Re_p in the range 140–160 and found the settling speed to increase by 12% with respect to the terminal velocity of an isolated particle for $Ga = 178$ and $\rho_p/\rho_f = 1.5$. This was due to clustering, which is in turn related to the steady oblique motion observed in this regime. Indeed, at $Ga < 155$ spheres fall straight and no clustering is observed, which has also been confirmed numerically by Zaidi et al. (2014). The behavior at higher volume fractions (from 9 to 35%), higher density ratios (between 2 and 5), but lower Ga (between 50 and 100) were investigated numerically by Willen & Prosperetti (2019), who observed a tendency toward particle clustering for $\rho_p/\rho_f > 3$ at the lower concentrations examined. These authors also confirmed the anisotropic nature of the particle velocity fluctuations and diffusivity in this parameter range. In the presence of the upward flow typical of fluidized-bed solid–liquid systems, simulations revealed the presence of continuity waves of the coarse-grained volume fractions, indicating the need to consider large enough systems to capture the macroscopic dynamics at higher concentrations.

4.1.2. Particle dynamics in homogeneous turbulence.

While the kinematics of small particles is dictated by their response time, for large particles their size compared to flow scales takes a more prominent and possibly leading role. In particular, the variance of the finite-size particle acceleration is related to that of the fluid pressure integrated over their surface (Qureshi et al. 2007). For neutrally buoyant particles in high-Re turbulence, Volk et al. (2011) confirmed that the particle acceleration variance scales as $D_p^{-2/3}$ (plus intermittency corrections) in the range $D_p/\eta = 1.6$–41, which is consistent with the scaling of pressure increments in Kolmogorov turbulence. These authors also showed the particle response time (taken as the decay time of the acceleration autocorrelation) to grow approximately linearly with D_p/η. This agreed with the later simulations of Uhlmann & Chouippe (2017). Qureshi et al. (2008) used helium-filled soap bubbles in air and varied both the particle size ($D_p/\eta = 13$–23) and the density ratio ($\rho_p/\rho_f = 1$–65), finding nonmonotonic trends of the acceleration variance. This contradicts both the heavy point-particle limit and the finite-size neutrally buoyant limit, demonstrating that the contributions of size and density to the particle response cannot be trivially absorbed in a single parameter. The limitations of the response time (and therefore the Stokes number) as the sole descriptor of finite-size particle dynamics also concern the collective behavior. Fiabane et al. (2012) found experimentally that large neutrally buoyant particles did not cluster. This contrasts with the results of Uhlmann & Chouippe (2017), who considered a similar range of parameters and did detect clustering. This, however, was only mild and not associated with preferential sampling of the strain/rotation field, as for point particles.

When finite-size particles settle in homogeneous turbulence (either sustained or decaying), nonlinear effects become relevant. Good et al. (2014) showed that reductions of the mean settling speed occur when the particle terminal velocity is larger than the turbulent velocity fluctuations. Particles are not able to side-step the turbulent eddies and fall almost vertically: Preferential sweeping is suppressed and mean settling reduces due to the drag increase at finite Re_p. The

reductions of the settling speed of finite-size particles are also related to nonlinear and unsteady drag in dilute conditions, despite the fact that hydrodynamic and particle–particle interactions cannot be neglected. Byron (2015) experimentally investigated the settling in turbulence of hydrogel particles the size of the Taylor microscale. She found that particles with a nominal settling velocity of the order of the fluid velocity fluctuations fell on average 40–60% slower than they did in quiescent fluid for $\rho_p/\rho_f \approx 1.02$. The same trend was found in the simulations by Fornari et al. (2016b,c) for $\rho_p/\rho_f = 1.02$, $D_p/\eta = 12$, and $Ga = 145$, with a reduction of settling speed of 12 and 14% for volume fraction 0.5 and 1%, respectively. This was explained by nonstationary effects related to vortex shedding, which increased the total drag by about 10–12%. This is consistent with the results of Homann et al. (2013), who found that the drag force on a stationary particle increases with the ambient turbulence intensity and Re_p. Decreasing Ga to 20, Fornari et al. (2016c) observed that the reduction of settling speed in turbulence reached 60%. In addition to unsteady effects, nonlinear effects come into play as an increase of the vertical drag induced by the particle horizontal motions. Y. Wang et al. (2019) reported significant lateral forces due to the combination of vortex shedding and the Magnus effect for a solid sphere free to rotate in a turbulent flow. Increasing Φ_V to 10%, Fornari et al. (2019) reported that the difference in mean settling speed between quiescent and turbulent background reduced to 1.7%, the process being mainly determined by the hindering effect. The collision frequency is larger in quiescent fluid than in turbulence for $\Phi_V = 0.5$–1% due to frequent DKT events, while the opposite is true at $\Phi_V = 5$–10% due to the larger relative velocities.

The effect of turbulence on particles with $Ga = 180$ and $\rho_p/\rho_f = 1.5$ was examined by Chouippe & Uhlmann (2019). Stronger turbulence inhibited wake-induced clustering but enhanced clustering by preferential sampling. These two effects combined reduced the settling speed to values of the order of the terminal velocity of an isolated particle in quiescent fluid.

4.1.3. Turbulence modulation.
Large particles with nominally identical τ_p (based on Stokes drag) but different size and density have different effects on isotropic turbulence (Lucci et al. 2011). The modulation of turbulence depends on a variety of factors; in particular, geometric effects become important for $D_p/\eta > 1$, leading to a spatial filtering of the turbulent structures (Naso & Prosperetti 2010). An increase of the energy dissipation rate and a decrease of the turbulence kinetic energy was first reported by Ten Cate et al. (2004) and Yeo et al. (2010) for large neutrally buoyant spheres. Bellani et al. (2012) showed that the energy content decreases at large scales and increases at small scales, consistent with the finding that particles transfer energy from large to small scales, as indicated by the dissipation spectra of Yeo et al. (2010). For Taylor-scale particles in decaying turbulence, Lucci et al. (2010) found that the turbulent kinetic energy was reduced and viscous dissipation was enhanced close to the particle front, an effect that increased with particle density. Gao et al. (2013) showed that the pivoting wavelength, where the particle-laden turbulence spectra intersect the single-phase one, is a function of the particle size, with steeper variations for smaller particles. For $D_p \approx \eta$, Schneiders et al. (2017) showed that spherical particles absorbed energy from the large scales of the carrier flow by inhibiting vortex-stretching. At small scales, the turbulent motion was determined by the inertial particle dynamics, as the rotational motion of the particles decoupled from the local flow when particle density increased.

In homogeneous shear turbulence, Tanaka & Teramoto (2015) and Yousefi et al. (2020) showed by PR-DNS that Taylor-scale particles attenuated the turbulent kinetic energy at lower volume fractions through the enhancement of the dissipation rate close to the surface of particles. Particles exhibit a weak tendency to accumulate in vortex layers where pair interactions induce vortices around the particle surface and regions of high Reynolds shear stress, resulting in a net enhancement of the turbulence activity above $\Phi_V = 10\%$.

These studies, however, neglected the effect of gravity, although the Galileo number can easily be $\mathcal{O}(100)$ in natural and industrial flows. In homogeneous turbulence, Fornari et al. (2019) found that the mean energy dissipation increased almost linearly with Φ_V at least up to 10%, leading to a large reduction of Re for $Ga = 145$. In vertically sheared turbulence laden with dilute particles of $Ga < 56$, Tanaka (2017) found that settling led to high Reynolds shear stress between counter-rotating trailing vortices behind the particles, whereas in the horizontally sheared case they were reduced in the wakes of particles.

Considering the rich physics at play, turbulence modulations by finite-size particles at higher concentrations deserve deeper investigation, in particular when settling is important. A promising approach is the analysis of the scale-by-scale budget of the turbulent kinetic energy, which lately facilitated significant physical insights in fiber suspensions (Olivieri et al. 2020) and bubbly flows (Pandey et al. 2020).

4.2. Wall-Bounded Turbulence

The presence of the wall introduces a no-slip no-penetration condition for the velocity field and an excluded volume for the particle, which can generally slide and roll on a wall. As for infinitesimal particles, below we discuss 2D plane channel and pipe flows, although more recent studies also consider more complex configurations.

4.2.1. Spatial distribution and migration.
Most recent studies on finite-size particle transport in wall-bounded turbulence consider relatively dense suspensions, with solid volume fractions ranging from a few percent to 30%. Motivated by industrial processes or natural phenomena such as sediment transport, these studies assume the liquid to be water and $\rho_p/\rho_f < 10$; neutrally buoyant particles are often considered to disentangle fundamental aspects of the problem.

The outer and inner (viscous) scales play different and equally important roles in wall turbulence. Therefore, the particle diameter is to be compared both to the channel height (or pipe diameter) and to the viscous length. Recent simulations consider particle size in inner units, $D_p^+ = 10\text{--}50$, which is characteristic of many industrial and natural settings. However, the present computational costs limit the flow Reynolds number and, therefore, particles are relatively large in outer units, typically 1/20 or at most 1/40 of the channel height.

The sketch in **Figure 6** reports the wall-normal particle distribution typically observed with neutrally buoyant finite-size spheres, as observed in experiments (Zade et al. 2018) and numerical simulations (Lashgari et al. 2016, 2017; Ardekani et al. 2018; Yousefi et al. 2021) for $\Phi_V > 10\%$. Two features characterize these profiles: the formation of a layer at the wall, whose thickness is slightly larger than the particle diameter, and the migration with a maximum in local volume fraction at the channel/pipe center. Similar profiles are observed for negatively buoyant particles, with increased concentration on the lower half and the peak at the upper wall disappearing. Note that the local volume fraction is usually calculated in wall-parallel slabs: It is therefore zero at the wall where the contact between spheres and wall reduces to single points.

The particle wall layer is due to the presence of a boundary that limits the volume available for the particle motion. A first layer of particles at the wall is in fact also observed in rheological studies and laminar flows (Yeo & Maxey 2010, Lashgari et al. 2014). Peng et al. (2019) considered rigid neutrally buoyant spheres at $\Phi_V = 5\%$, artificially removed particle rotation, and observed the particle wall layer to disappear. These authors attributed the formation of the layer to the balance between a strong lubrication force driving the particles away from the wall and an opposite lift force due to the particle rotation and the local mean shear. The local minimum of particle concentration, approximately one diameter away from the wall, was related to the change of sign
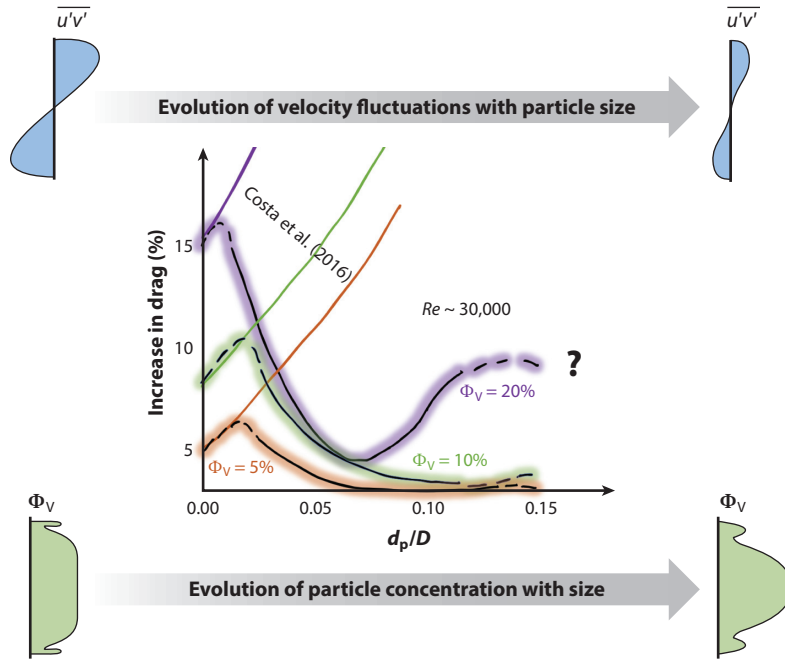
Figure 6

Turbulent pipe flow of almost neutrally buoyant finite-size spheres. When increasing the particle volume fraction Φ_V, we observe the formation of a particle wall layer and, later, accumulation toward the pipe core (*bottom arrow*). Correspondingly, the Reynolds stresses decrease due to turbulence quenching in the densely packed core, reducing velocity fluctuations $\overline{u'v'}$ (*top arrow*). These effects combine to give the nonmonotonic behavior of the percentage drag modifications (*middle plot*) (Zade et al. 2018), which can be predicted by the theory of Costa et al. (2016) (*thin solid lines*) as long as the concentration away from the walls can be assumed to be uniform.

of the fluid–particle relative motion, which reverses the direction of the lift force. Results for larger particles and semidense conditions ($\Phi_V = 10$–20%) indicated that particle migration is rooted in the particle collisions, which are more frequent in regions of larger shear where eventually the concentration has a minimum (Fornari et al. 2016a); the near-wall concentration peak was found to increase with the fluid and particle inertia (Ardekani et al. 2018). Due to the different boundary conditions, particle and fluid velocity differ in this thin wall layer. The existence of a slip velocity invalidates rheological models based on an effective viscosity and demands more complex, two-fluid models (see, among others, Municchi et al. 2019).

The scenario is different in dilute conditions. In turbulent channel flows, finite-size particles with $D_p^+ \lesssim 10$ were found to preferentially accumulate in low-speed streaks. This was observed in PR-DNS simulations of both heavy (Kidanemariam et al. 2013) and neutrally buoyant particles (Wang et al. 2018). The particle–wall interaction was studied by Baker & Coletti (2021) through time-resolved PIV/PTV for $D_p^+ = 16$ and $\rho_p/\rho_f = 1.02$. The concentration profiles followed a power law with a shallower slope than that predicted by Rouse–Prandtl theory, with no evidence of turbophoresis. The particles that came in contact with the wall (a small fraction of the total) traveled faster than the local fluid, both before reaching the wall and after leaving it. Therefore, they were decelerated by drag and pushed downward by shear-induced lift. The duration of the contact with the wall had a characteristic time close to τ_p, consistent with measurements from Ebrahimian et al. (2019) for $D_p^+ = 6.8$ and $\rho_p/\rho_f = 2.5$. In the PR-DNS simulations of Costa et al.

(2020) ($D_{\mathrm{p}}^{+} = 3$ and $\rho_{\mathrm{p}}/\rho_{\mathrm{f}} = 100$, but with zero gravity), the particle residence time in the viscous sublayer was also of order τ_{p}.

The available experimental and numerical data on particle migration toward the channel center indicate that the peak in concentration at the centerline appears for nominal solid volume fractions above 10% and its amplitude is weakly decreasing with Re. Particle migration toward the centerline increases with Φ_{V}, which may be related to increased collision rates. It also increases with D_{p} and $\rho_{\mathrm{p}}/\rho_{\mathrm{f}}$ and, hence, particle inertia; however, it decreases with Re due to the larger turbulent mixing. Migration toward the centerline was found in laminar flows only for $\Phi_{\mathrm{V}} \gtrsim 30\%$; below this threshold, the maximum local volume fraction was attained between the wall and the centerline, which is reminiscent of the Segre–Silberberg effect (Matas et al. 2004).

4.2.2. Turbulent modulation and drag.

For neutrally buoyant particles, the particle distribution just described has a threefold effect on the underlying turbulence: On the one hand, the wall layer increases the overall drag due to increased friction at the wall; on the other hand, the particle-dense core region quenches turbulent fluctuations and the associated turbulent transport. At the same time, particle stresses increase with the local concentration, increasing the total drag. These three effects balance each other, and experiments showed that, surprisingly, the total drag stays within 5–10% of that of the single-phase flow over a range of particle sizes and flow Reynolds number (Zade et al. 2018, Zade 2019).

To quantify and predict the role of particles on the turbulence dynamics, researchers have proposed two approaches to extract relevant information from numerical simulations. Following Zhang & Prosperetti (2010), Picano et al. (2015) considered the average momentum transfer across the channel. Three contributions were identified: viscous stresses, Reynolds stresses related to fluid and particle velocity correlations, and particle stresses. Due to the intrinsic features of the numerical algorithms adopted for interface-resolved simulations, the last contribution consists of the resistance of the rigid particles to flow-induced deformations, but also of forces arising from particle collisions and viscous lubrication corrections, which are numerically treated as additional interaction forces. Alternatively, one can resort to the turbulent kinetic energy budget (Ardekani & Brandt 2019). In this case, in addition to the classic production by mean shear, viscous dissipation, and spatial fluxes (integrating to zero) in the fluid phase, one obtains an interphase energy injection term (Tanaka & Teramoto 2015).

Costa et al. (2016) showed that for particles larger than the smallest turbulence scales, the suspension flow cannot be described by means of an effective suspension viscosity. This was attributed to the formation of the particle wall layer and the associated slip velocity. As shown by Costa et al. (2018), the increased dissipation is associated with hot spots of high wall-shear stress due to the strong velocity gradients between rotating particles. This corresponds to increased viscous and particle stresses and a positive peak of the interphase energy injection near the wall. By assuming two distinct transport mechanisms in the wall layer and for the turbulence in the bulk, these authors defined a virtual wall location such that the flow in the bulk can still be accurately described by an effective suspension viscosity; this enabled them to predict scaling laws for the mean velocity profile and the increase in drag as a function of the particle size and volume fraction. The model of Costa et al. (2016) implied that the drag is always larger in the presence of spherical particles. It fails, however, for high Re and $D_{\mathrm{p}}^{+} > 20$ because it does not consider particle accumulation at the centerline.

Particle rotation rates in the near-wall region and the boundary condition for the fluid velocity play an important role for the flow dynamics. It was observed that increasing the particle moment of inertia by a factor of 20 at fixed size and weight lowered the particle angular velocity, decreased the turbulence intensity close to the wall, and reduced the drag, which is consistent

with the abovementioned findings of Peng et al. (2019). In the case of an elastic wall, Ardekani et al. (2019) observed that the velocity fluctuations at the interface between the fluid and the elastic material push the particles toward the channel core, reducing the drag in comparison to the single-phase flow over the same deformable wall. A similar behavior was observed for neutrally buoyant particles transported over porous walls, when wall-normal fluctuations at the porous interface are not zero (S. Abtahi, M.E. Rosti, L. Brandt & P. Mirbod, manuscript in preparation). Interestingly, altering the near-wall dynamics with roughness and porosity might reduce the drag in particle-laden turbulence, in contrast to the case of single-phase turbulence.

Leaving the wall, the migration toward the pipe/channel core also has a significant effect on the global suspension behavior. In this region, large particles are densely packed and move as a compact aggregate with small relative velocities, and the level of turbulent fluctuations significantly decreases (Lashgari et al. 2016, Ardekani et al. 2018). This greatly reduces particle dispersion and mixing in the flow. One potentially important consequence is the reduction of heat transfer in particle suspensions: Yousefi et al. (2021) performed simulations of heat transfer in particulate plane channel flows and reported an increase of turbulent mixing for moderate volume fractions, as well as a decrease below the values measured in single-phase turbulence for solid volume fractions around 30%, when fluctuations are quenched at the core. Note, however, that the reduction of turbulent fluctuations and Reynolds stresses is not necessarily associated with reduced drag. Indeed, numerical simulations showed that particle stresses increase when particles migrate toward the channel core. These competing effects lead to a nonmonotonic behavior of the drag versus the Reynolds number or the particle size (Zade et al. 2018). In particular, smaller particles increase the drag due to the formation of the particle wall layer. Increasing the particle size, these start to accumulate toward the channel center and the drag decreases due to turbulence attenuation. Further increasing the particle size, turbulence is further attenuated, whereas particle stresses increase in the bulk, where they accumulate. However, despite the increased particle stresses, the total drag decreases to values of the order of or slightly below that of the single-phase flow (see **Figure 6**).

In internal flows, dense suspensions of negatively buoyant, finite-size particles produce several dense layers adjacent to the wall (Shao et al. 2012; Zade et al. 2018, 2019; Baker & Coletti 2019). These slide on top of each other, resulting in a quasi-linear particle velocity profile. The turbulence activity is dampened within the dense layers, while it is enhanced above them. This is partly due to the propagation of vortices shed by the layers into the bulk flow, and partly due to the strong mean shear that the particles imprint on the fluid, greatly amplifying the production of turbulent kinetic energy.

SUMMARY POINTS

1. Experiments that simultaneously image both dispersed and carrier phases are providing novel insights into mechanisms long theorized or simulated with simplistic assumptions. Numerical advances and ever-increasing supercomputing capabilities have enabled fully resolved simulations of large numbers of small particles that appeared unthinkable a decade ago. Further breakthroughs in our understanding of particle-laden turbulence will come from the synergistic application of both approaches.

2. Gravity plays a significant role in most practical applications. It couples nontrivially with inertia and sometimes has an opposite effect on, for example, particle dispersion and acceleration. Therefore, conclusions drawn in zero gravity should not be extrapolated outside of this condition.

3. Inertial clustering occurs over a wide portion of the parameter space, far beyond the conditions for which preferential sampling is realized. In high-*Re* turbulence, clusters have size distributions spanning orders of magnitude. While the precise mechanisms behind their formation are still debated and may be problem dependent, history effects become prominent as inertia and gravitational drift increase.

4. For particles larger than the minimal flow scales, the roles of size and density are distinct and cannot be absorbed in the response time alone. The geometric effects can dominate the fluctuating energy of the flow compared to the background turbulence, especially for dense particles with significant slip velocity relative to the fluid.

5. While turbulence can greatly enhance the settling of small particles via preferential sweeping, the opposite is true for large particles over a sizeable portion of the parameter space. This is owing to unsteady and nonlinear effects. The dependence on volume fraction is complex due to competing effects of collective drag, hydrodynamic interactions, and hindrance by the displaced fluid.

6. Wall turbulence is significantly altered by the migration and accumulation of finite-size particles. While the particle wall layer increases drag owing to larger friction, packing of neutrally buoyant particles in the core region quenches turbulence activity. This leads to increased mixing in the near-wall region and a pseudo-laminar flow in the core.

FUTURE ISSUES

1. Today, the research field is divided between studies of small heavy particles and of large weakly buoyant particles. Bridging this gap will require both simulations and experiments to surpass present limitations on the minimum particle size and maximum concentration, respectively. The expected dividends are large considering the practical importance of the regimes that would become accessible.

2. Point-particle models remain the method of choice for high–Reynolds number simulations of small particles, but their quantitative agreement with experiments is still unsatisfactory regarding both transport and turbulence modification. Progress in this area hinges on the accurate representation of the various forces acting on nonisolated particles in turbulence, and on one-to-one comparisons between simulations and experiments.

3. Validation of particle-resolved direct numerical simulations (PR-DNS) is also necessary before it can be used as ground truth to inform lower-order models. Improvements in the spatiotemporal resolution and accuracy of experimental measurements are needed to capture the fluid dynamics around submillimeter particles.

4. Large-scale experiments and simulations in single-phase flows need to be paralleled by similar efforts in particle-laden conditions. Field measurements of natural flows, whose exploration marked major successes of classic turbulence theory, offer unique opportunities to probe otherwise unattainable regimes.

5. Three-dimensional imaging techniques have seen tremendous progress in recent years, but the rewards for the characterization of inertial particle dynamics are still to be reaped. The ability to track individual particles at higher-than-ever concentrations has been the most notable recent trend and will be an asset for this field.

6. To extend the range of applicability of PR-DNS in dense regimes, it is crucial to correctly include short-range interactions: friction, attractive/repulsive forces, collision-coalescence, breakup, and lubrication forces. This requires a closer collaboration with experimentalists.

DISCLOSURE STATEMENT

ACKNOWLEDGMENTS

LITERATURE CITED

Adrian L, Adrian RJ, Westerweel J. 2011. *Particle Image Velocimetry*. Cambridge, UK: Cambridge Univ. Press

Akiki G, Moore W, Balachandar S. 2017. Pairwise-interaction extended point-particle model for particle-laden flows. *J. Comput. Phys.* 351:329–57

Aliseda A, Cartellier A, Hainaux F, Lasheras JC. 2002. Effect of preferential concentration on the settling velocity of heavy particles in homogeneous isotropic turbulence. *J. Fluid Mech.* 468:77–105

Aliseda A, Lasheras J. 2011. Preferential concentration and rise velocity reduction of bubbles immersed in a homogeneous and isotropic turbulent flow. *Phys. Fluids* 23(9):093301

Ardekani MN, Al Asmar L, Picano F, Brandt L. 2018. Numerical study of heat transfer in laminar and turbulent pipe flow with finite-size spherical particles. *Int. J. Heat Fluid Flow* 71:189–99

Ardekani MN, Brandt L. 2019. Turbulence modulation in channel flow of finite-size spheroidal particles. *J. Fluid Mech.* 859:887–901

Ardekani MN, Rosti ME, Brandt L. 2019. Turbulent flow of finite-size spherical particles in channels with viscous hyper-elastic walls. *J. Fluid Mech.* 873:410–40

Baker LJ, Coletti F. 2019. Experimental study of negatively buoyant finite-size particles in a turbulent boundary layer up to dense regimes. *J. Fluid Mech.* 866:598–629

Baker LJ, Coletti F. 2021. Particle–fluid–wall interaction of inertial spherical particles in a turbulent boundary layer. *J. Fluid Mech.* 908:A39

Baker LJ, Frankel A, Mani A, Coletti F. 2017. Coherent clusters of inertial particles in homogeneous turbulence. *J. Fluid Mech.* 833:364–98

Balachandar S, Eaton JK. 2010. Turbulent dispersed multiphase flow. *Annu. Rev. Fluid Mech.* 42:111–33

Balachandar S, Liu K, Lakhote M. 2019. Self-induced velocity correction for improved drag estimation in Euler–Lagrange point-particle simulations. *J. Comput. Phys.* 376:160–85

Balachandar S, Moore W, Akiki G, Liu K. 2020. Toward particle-resolved accuracy in Euler–Lagrange simulations of multiphase flow using machine learning and pairwise interaction extended point-particle (PIEP) approximation. *Theor. Comput. Fluid Dyn.* 34(4):401–28

Banko AJ, Villafañe L, Kim JH, Eaton JK. 2020. Temperature statistics in a radiatively heated particle-laden turbulent square duct flow. *Int. J. Heat Fluid Flow* 84:108618

Battista F, Mollicone JP, Gualtieri P, Messina R, Casciola CM. 2019. Exact regularized point particle (ERPP) method for particle-laden wall-bounded flows in the two-way coupling regime. *J. Fluid Mech.* 878:420–44

Beals MJ, Fugal JP, Shaw RA, Lu J, Spuler SM, Stith JL. 2015. Holographic measurements of inhomogeneous cloud mixing at the centimeter scale. *Science* 350(6256):87–90

Bec J. 2003. Fractal clustering of inertial particles in random flows. *Phys. Fluids* 15(11):L81–84

Bec J, Biferale L, Boffetta G, Cencini M, Musacchio S, Toschi F. 2006. Lyapunov exponents of heavy particles in turbulence. *Phys. Fluids* 18(9):091702

Bec J, Biferale L, Cencini M, Lanotte A, Musacchio S, Toschi F. 2007. Heavy particle concentration in turbulence at dissipative and inertial scales. *Phys. Rev. Lett.* 98(8):084502

Bec J, Biferale L, Lanotte A, Scagliarini A, Toschi F. 2010. Turbulent pair dispersion of inertial particles. *J. Fluid Mech.* 645:497–528

Bec J, Homann H, Ray SS. 2014. Gravity-driven enhancement of heavy particle clustering in turbulent flow. *Phys. Rev. Lett.* 112(18):184501

Bellani G, Byron ML, Collignon AG, Meyer CR, Variano EA. 2012. Shape effects on turbulent modulation by large nearly neutrally buoyant particles. *J. Fluid Mech.* 712:41–60

Benson M, Tanaka T, Eaton JK. 2005. Effects of wall roughness on particle velocities in a turbulent channel flow. *J. Fluids Eng.* 127(2):250–56

Bergougnoux L, Bouchet G, Lopez D, Guazzelli E. 2014. The motion of solid spherical particles falling in a cellular flow field at low Stokes number. *Phys. Fluids* 26(9):093302

Berk T, Coletti F. 2020. Transport of inertial particles in high-Reynolds-number turbulent boundary layers. *J. Fluid Mech.* 903:A18

Berk T, Coletti F. 2021. Dynamics of small heavy particles in homogeneous turbulence: a Lagrangian experimental study. *J. Fluid Mech.* 917:A47

Bernardini M. 2014. Reynolds number scaling of inertial particle statistics in turbulent channel flows. *J. Fluid Mech.* 758:R1

Bosse T, Kleiser L, Meiburg E. 2006. Small particles in homogeneous turbulence: settling velocity enhancement by two-way coupling. *Phys. Fluids* 18(2):027102

Bragg AD, Collins LR. 2014. New insights from comparing statistical theories for inertial particles in turbulence: I. Spatial distribution of particles. *New J. Phys.* 16(5):055013

Bragg AD, Ireland PJ, Collins LR. 2016. Forward and backward in time dispersion of fluid and inertial particles in isotropic turbulence. *Phys. Fluids* 28(1):013305

Byron M. 2015. *The rotation and translation of non-spherical particles in homogeneous isotropic turbulence.* PhD Thesis, Univ. Calif., Berkeley

Capecelatro J, Desjardins O. 2013. An Euler–Lagrange strategy for simulating particle-laden flows. *J. Comput. Phys.* 238:1–31

Capecelatro J, Desjardins O. 2015. Mass loading effects on turbulence modulation by particle clustering in dilute and moderately dilute channel flows. *J. Fluids Eng.* 137(11):111102

Capecelatro J, Desjardins O, Fox RO. 2015. On fluid–particle dynamics in fully developed cluster-induced turbulence. *J. Fluid Mech.* 780:578–635

Carter D, Hassaini R, Eshraghi J, Vlachos P, Coletti F. 2020. Multi-scale imaging of upward liquid spray in the far-field region. *Int. J. Multiph. Flow* 132:103430

Chen L, Goto S, Vassilicos J. 2006. Turbulent clustering of stagnation points and inertial particles. *J. Fluid Mech.* 553:143–54

Chouippe A, Uhlmann M. 2019. On the influence of forced homogeneous-isotropic turbulence on the settling and clustering of finite-size particles. *Acta Mech.* 230(2):387–412

Coleman S, Vassilicos J. 2009. A unified sweep-stick mechanism to explain particle clustering in two-and three-dimensional homogeneous, isotropic turbulence. *Phys. Fluids* 21(11):113301

Costa P, Brandt L, Picano F. 2020. Interface-resolved simulations of small inertial particles in turbulent channel flow. *J. Fluid Mech.* 883:A54

Costa P, Brandt L, Picano F. 2021. Near wall turbulence modulation by small inertial particles. *J. Fluid Mech.* 922:A9

Costa P, Picano F, Brandt L, Breugem WP. 2016. Universal scaling laws for dense particle suspensions in turbulent wall-bounded flows. *Phys. Rev. Lett.* 117(13):134501

Costa P, Picano F, Brandt L, Breugem WP. 2018. Effects of the finite particle size in turbulent wall-bounded flows of dense suspensions. *J. Fluid Mech.* 843:450–78

Csanady G. 1963. Turbulent diffusion of heavy particles in the atmosphere. *J. Atmos. Sci.* 20(3):201–8

Daitche A, Tél T. 2011. Memory effects are relevant for chaotic advection of inertial particles. *Phys. Rev. Lett.* 107(24):244501

Discetti S, Coletti F. 2018. Volumetric velocimetry for fluid flows. *Meas. Sci. Technol.* 29(4):042001

Eaton JK. 2009. Two-way coupled turbulence simulations of gas-particle flows using point-particle tracking. *Int. J. Multiph. Flow* 35(9):792–800

Ebrahimian M, Sanders RS, Ghaemi S. 2019. Dynamics and wall collision of inertial particles in a solid–liquid turbulent channel flow. *J. Fluid Mech.* 881:872–905

Elghobashi S. 1994. On predicting particle-laden turbulent flows. *Appl. Sci. Res.* 52(4):309–29

Esmaily M, Horwitz J. 2018. A correction scheme for two-way coupled point-particle simulations on anisotropic grids. *J. Comput. Phys.* 375:960–82

Ferenc JS, Néda Z. 2007. On the size distribution of Poisson Vorono cells. *Physica A* 385(2):518–26

Fessler JR, Kulick JD, Eaton JK. 1994. Preferential concentration of heavy particles in a turbulent channel flow. *Phys. Fluids* 6(11):3742–49

Février P, Simonin O, Squires KD. 2005. Partitioning of particle velocities in gas-solid turbulent flows into a continuous field and a spatially uncorrelated random distribution: theoretical formalism and numerical study. *J. Fluid Mech.* 533:1–46

Fiabane L, Zimmermann R, Volk R, Pinton JF, Bourgoin M. 2012. Clustering of finite-size particles in turbulence. *Phys. Rev. E* 86(3):035301

Fong KO, Amili O, Coletti F. 2019. Velocity and spatial distribution of inertial particles in a turbulent channel flow. *J. Fluid Mech.* 872:367–406

Fornari W, Formenti A, Picano F, Brandt L. 2016a. The effect of particle density in turbulent channel flow laden with finite size particles in semi-dilute conditions. *Phys. Fluids* 28(3):033301

Fornari W, Picano F, Brandt L. 2016b. Sedimentation of finite-size spheres in quiescent and turbulent environments. *J. Fluid Mech.* 788:640–69

Fornari W, Picano F, Sardina G, Brandt L. 2016c. Reduced particle settling speed in turbulence. *J. Fluid Mech.* 808:153–67

Fornari W, Zade S, Brandt L, Picano F. 2019. Settling of finite-size particles in turbulence at different volume fractions. *Acta Mech.* 230(2):413–30

Forterre Y, Pouliquen O. 2008. Flows of dense granular media. *Annu. Rev. Fluid Mech.* 40:1–24

Fortes AF, Joseph DD, Lundgren TS. 1987. Nonlinear mechanics of fluidization of beds of spherical particles. *J. Fluid Mech.* 177:467–83

Frankel A, Pouransari H, Coletti F, Mani A. 2016. Settling of heated particles in homogeneous turbulence. *J. Fluid Mech.* 792:869–93

Fullmer WD, Hrenya CM. 2017. The clustering instability in rapid granular and gas-solid flows. *Annu. Rev. Fluid Mech.* 49:485–510

Gao H, Li H, Wang LP. 2013. Lattice Boltzmann simulation of turbulent flow laden with finite-size particles. *Comput. Math. Appl.* 65(2):194–210

Gatignol R. 1983. The Faxen formulae for a rigid particle in an unsteady non-uniform Stokes flow. *J. Mec. Theor. Appl.* 2(2):143–60

Gerashchenko S, Sharp N, Neuscamman S, Warhaft Z. 2008. Lagrangian measurements of inertial particle accelerations in a turbulent boundary layer. *J. Fluid Mech.* 617:255–81

Gibert M, Xu H, Bodenschatz E. 2010. Inertial effects on two-particle relative dispersion in turbulent flows. *EPL* 90(6):64005

Gibert M, Xu H, Bodenschatz E. 2012. Where do small, weakly inertial particles go in a turbulent flow? *J. Fluid Mech.* 698:160–67

Gondret P, Lance M, Petit L. 2002. Bouncing motion of spherical particles in fluids. *Phys. Fluids* 14(2):643–52

Good G, Gerashchenko S, Warhaft Z. 2012. Intermittency and inertial particle entrainment at a turbulent interface: the effect of the large-scale eddies. *J. Fluid Mech.* 694:371–98

Good G, Ireland P, Bewley G, Bodenschatz E, Collins L, Warhaft Z. 2014. Settling regimes of inertial particles in isotropic turbulence. *J. Fluid Mech.* 759:R3

Gualtieri P, Picano F, Casciola C. 2009. Anisotropic clustering of inertial particles in homogeneous shear flow. *J. Fluid Mech.* 629:25–39

Gualtieri P, Picano F, Sardina G, Casciola CM. 2015. Exact regularized point particle method for multiphase flows in the two-way coupling regime. *J. Fluid Mech.* 773:520–61

Guazzelli E, Morris JF. 2012. *A Physical Introduction to Suspension Dynamics*. Cambridge, UK: Cambridge Univ. Press

Gustavsson K, Mehlig B. 2016. Statistical models for spatial patterns of heavy particles in turbulence. *Adv. Phys.* 65(1):1–57

Haller G, Sapsis T. 2008. Where do inertial particles go in fluid flows? *Physica D* 237(5):573–83

Homann H, Bec J, Grauer R. 2013. Effect of turbulent fluctuations on the drag and lift forces on a towed sphere and its boundary layer. *J. Fluid Mech.* 721:155–79

Horne WJ, Mahesh K. 2019. A massively-parallel, unstructured overset method to simulate moving bodies in turbulent flows. *J. Comput. Phys.* 397:108790

Horowitz M, Williamson C. 2010. The effect of Reynolds number on the dynamics and wakes of freely rising and falling spheres. *J. Fluid Mech.* 651:251

Horwitz JAK, Iaccarino G, Eaton JK, Mani A. 2020. The discrete Green's function paradigm for two-way coupled Euler-Lagrange simulation. arXiv:2004.08480 [physics.flu-dyn]

Horwitz JAK, Mani A. 2016. Accurate calculation of Stokes drag for point–particle tracking in two-way coupled flows. *J. Comput. Phys.* 318:85–109

Horwitz JAK, Mani A. 2018. Correction scheme for point-particle models applied to a nonlinear drag law in simulations of particle-fluid interaction. *Int. J. Multiph. Flow* 101:74–84

Huck PD, Bateson C, Volk R, Cartellier A, Bourgoin M, Aliseda A. 2018. The role of collective effects on settling velocity enhancement for inertial particles in turbulence. *J. Fluid Mech.* 846:1059–75

Hunt J, Wray A, Moin P. 1988. Eddies, stream, and convergence zones in turbulent flows. In *Proceedings of the Summer Program 1988*, pp. 193–208. Stanford, CA: Cent. Turbul. Res.

Ijzermans RH, Meneguz E, Reeks MW. 2010. Segregation of particles in incompressible random flows: singularities, intermittency and random uncorrelated motion. *J. Fluid Mech.* 653:99–136

Ireland PJ. 2015. *Computational investigation of the effect of turbulence, inertia, and gravity on particle dynamics*. PhD Thesis, Cornell Univ., Ithaca, NY

Ireland PJ, Bragg AD, Collins LR. 2016a. The effect of Reynolds number on inertial particle dynamics in isotropic turbulence. Part 1. Simulations without gravitational effects. *J. Fluid Mech.* 796:617–58

Ireland PJ, Bragg AD, Collins LR. 2016b. The effect of Reynolds number on inertial particle dynamics in isotropic turbulence. Part 2. Simulations with gravitational effects. *J. Fluid Mech.* 796:659–711

Ireland PJ, Desjardins O. 2017. Improving particle drag predictions in Euler–Lagrange simulations with two-way coupling. *J. Comput. Phys.* 338:405–30

Ivey G, Winters K, Koseff J. 2008. Density stratification, turbulence, but how much mixing? *Annu. Rev. Fluid Mech.* 40:169–84

Jenny M, Dusek J, Bouchet G. 2004. Instabilities and transition of a sphere falling or ascending freely in a Newtonian fluid. *J. Fluid Mech.* 508:201–39

Khalitov D, Longmire EK. 2002. Simultaneous two-phase PIV by two-parameter phase discrimination. *Exp. Fluids* 32(2):252–68

Kidanemariam AG, Chan-Braun C, Doychev T, Uhlmann M. 2013. Direct numerical simulation of horizontal open channel flow with finite-size, heavy particles at low solid volume fraction. *New J. Phys.* 15(2):025031

Kiger K, Pan C. 2000. PIV technique for the simultaneous measurement of dilute two-phase flows. *J. Fluids Eng.* 122(4):811–18

Koblitz A, Lovett S, Nikiforakis N, Henshaw WD. 2017. Direct numerical simulation of particulate flows with an overset grid method. *J. Comput. Phys.* 343:414–31

Kuerten JG. 2016. Point-particle DNS and LES of particle-laden turbulent flow: a state-of-the-art review. *Flow Turbul. Combust.* 97(3):689–713

Kuerten JG, Vreman A. 2015. Effect of droplet interaction on droplet-laden turbulent channel flow. *Phys. Fluids* 27(5):053304

Lashgari I, Picano F, Breugem WP, Brandt L. 2014. Laminar, turbulent, and inertial shear-thickening regimes in channel flow of neutrally buoyant particle suspensions. *Phys. Rev. Lett.* 113(25):254502

Lashgari I, Picano F, Breugem WP, Brandt L. 2016. Channel flow of rigid sphere suspensions: particle dynamics in the inertial regime. *Int. J. Multiph. Flow* 78:12–24

Lashgari I, Picano F, Costa P, Breugem WP, Brandt L. 2017. Turbulent channel flow of a dense binary mixture of rigid particles. *J. Fluid Mech.* 818:623–45

Lavezzo V, Soldati A, Gerashchenko S, Warhaft Z, Collins L. 2010. On the role of gravity and shear on inertial particle accelerations in near-wall turbulence. *J. Fluid Mech.* 658:229–46

Lee J, Lee C. 2019. The effect of wall-normal gravity on particle-laden near-wall turbulence. *J. Fluid Mech.* 873:475–507

Li C, Lim K, Berk T, Abraham A, Heisel M, et al. 2021. Settling and clustering of snow particles in atmospheric turbulence. *J. Fluid Mech.* 912:A49

Li J, Wang H, Liu Z, Chen S, Zheng C. 2012. An experimental study on turbulence modification in the near-wall boundary layer of a dilute gas-particle channel flow. *Exp. Fluids* 53(5):1385–403

Ling Y, Parmar M, Balachandar S. 2013. A scaling analysis of added-mass and history forces and their coupling in dispersed multiphase flows. *Int. J. Multiph. Flow* 57:102–14

Liu Y, Shen L, Zamansky R, Coletti F. 2020. Life and death of inertial particle clusters in turbulence. *J. Fluid Mech.* 902:R1

Lucci F, Ferrante A, Elghobashi S. 2010. Modulation of isotropic turbulence by particles of Taylor length-scale size. *J. Fluid Mech.* 650:5–55

Lucci F, Ferrante A, Elghobashi S. 2011. Is Stokes number an appropriate indicator for turbulence modulation by particles of Taylor-length-scale size? *Phys. Fluids* 23(2):025101

Marchioli C, Fantoni M, Soldati A. 2007. Influence of added mass on anomalous high rise velocity of light particles in cellular flow field: a note on the paper by Maxey (1987). *Phys. Fluids* 19(9):098101

Marchioli C, Soldati A. 2002. Mechanisms for particle transfer and segregation in a turbulent boundary layer. *J. Fluid Mech.* 468:283–315

Matas JP, Morris JF, Guazzelli É. 2004. Inertial migration of rigid spherical particles in Poiseuille flow. *J. Fluid Mech.* 515:171–95

Mathai V, Lohse D, Sun C. 2020. Bubbly and buoyant particle–laden turbulent flows. *Annu. Rev. Condens. Matter Phys.* 11:529–59

Maxey MR. 1987. The gravitational settling of aerosol particles in homogeneous turbulence and random flow fields. *J. Fluid Mech.* 174:441–65

Maxey MR. 2017. Simulation methods for particulate flows and concentrated suspensions. *Annu. Rev. Fluid Mech.* 49:171–93

Maxey MR, Riley JJ. 1983. Equation of motion for a small rigid sphere in a nonuniform flow. *Phys. Fluids* 26(4):883–89

Mehrabadi M, Horwitz J, Subramaniam S, Mani A. 2018. A direct comparison of particle-resolved and point-particle methods in decaying turbulence. *J. Fluid Mech.* 850:336–69

Mehrabadi M, Tenneti S, Garg R, Subramaniam S. 2015. Pseudo-turbulent gas-phase velocity fluctuations in homogeneous gas-solid flow: fixed particle assemblies and freely evolving suspensions. *J. Fluid Mech.* 770:210–46

Momenifar M, Bragg AD. 2020. Local analysis of the clustering, velocities, and accelerations of particles settling in turbulence. *Phys. Rev. Fluids* 5(3):034306

Monchaux R. 2012. Measuring concentration with Vorono diagrams: the study of possible biases. *New J. Phys.* 14(9):095013

Monchaux R, Bourgoin M, Cartellier A. 2010. Preferential concentration of heavy particles: a Vorono analysis. *Phys. Fluids* 22(10):103304

Monchaux R, Bourgoin M, Cartellier A. 2012. Analyzing preferential concentration and clustering of inertial particles in turbulence. *Int. J. Multiph. Flow* 40:1–18

Municchi F, Nagrani PP, Christov IC. 2019. A two-fluid model for numerical simulation of shear-dominated suspension flows. *Int. J. Multiph. Flow* 120:103079

Naso A, Prosperetti A. 2010. The interaction between a solid particle and a turbulent flow. *New J. Phys.* 12(3):033040

Nemes A, Dasari T, Hong J, Guala M, Coletti F. 2017. Snowflakes in the atmospheric surface layer: observation of particle-turbulence dynamics. *J. Fluid Mech.* 814:592–613

Nilsen C, Andersson HI, Zhao L. 2013. A Vorono analysis of preferential concentration in a vertical channel flow. *Phys. Fluids* 25(11):115108

Niño Y, Garcia M. 1996. Experiments on particle–turbulence interactions in the near–wall region of an open channel flow: implications for sediment transport. *J. Fluid Mech.* 326:285–319

Olivieri S, Brandt L, Rosti ME, Mazzino A. 2020. Dispersed fibers change the classical energy budget of turbulence via nonlocal transfer. *Phys. Rev. Lett.* 125(11):114501

Olivieri S, Picano F, Sardina G, Iudicone D, Brandt L. 2014. The effect of the Basset history force on particle clustering in homogeneous and isotropic turbulence. *Phys. Fluids* 26(4):041704

Ouellette NT, Xu H, Bodenschatz E. 2006. A quantitative study of three-dimensional Lagrangian particle tracking algorithms. *Exp. Fluids* 40(2):301–13

Pakseresht P, Esmaily M, Apte SV. 2020. A correction scheme for wall-bounded two-way coupled point-particle simulations. *J. Comput. Phys.* 420:109711

Pandey V, Ramadugu R, Perlekar P. 2020. Liquid velocity fluctuations and energy spectra in three-dimensional buoyancy-driven bubbly flows. *J. Fluid Mech.* 884:R6

Peng C, Ayala OM, Wang LP. 2019. A direct numerical investigation of two-way interactions in a particle-laden turbulent channel flow. *J. Fluid Mech.* 875:1096–144

Petersen AJ, Baker L, Coletti F. 2019. Experimental study of inertial particles clustering and settling in homogeneous turbulence. *J. Fluid Mech.* 864:925–70

Picano F, Breugem WP, Brandt L. 2015. Turbulent channel flow of dense suspensions of neutrally buoyant spheres. *J. Fluid Mech.* 764:463–87

Picciotto M, Marchioli C, Soldati A. 2005. Characterization of near-wall accumulation regions for inertial particles in turbulent boundary layers. *Phys. Fluids* 17(9):098101

Poelma C, Ooms G. 2006. Particle-turbulence interaction in a homogeneous, isotropic turbulent suspension. *Appl. Mech. Rev.* 59(2):78–90

Poelma C, Westerweel J, Ooms G. 2007. Particle–fluid interactions in grid-generated turbulence. *J. Fluid Mech.* 589:315–51

Prasath SG, Vasan V, Govindarajan R. 2019. Accurate solution method for the Maxey–Riley equation, and the effects of Basset history. *J. Fluid Mech.* 868:428–60

Pumir A, Wilkinson M. 2016. Collisional aggregation due to turbulence. *Annu. Rev. Condens. Matter Phys.* 7:141–70

Qureshi NM, Arrieta U, Baudet C, Cartellier A, Gagne Y, Bourgoin M. 2008. Acceleration statistics of inertial particles in turbulent flow. *Eur. Phys. J. B* 66(4):531–36

Qureshi NM, Bourgoin M, Baudet C, Cartellier A, Gagne Y. 2007. Turbulent transport of material particles: an experimental study of finite size effects. *Phys. Rev. Lett.* 99(18):184502

Richter DH, Sullivan PP. 2014. Modification of near-wall coherent structures by inertial particles. *Phys. Fluids* 26(10):103304

Risso F. 2018. Agitation, mixing, and transfers induced by bubbles. *Annu. Rev. Fluid Mech.* 50:25–48

Rosa B, Pozorski J, Wang LP. 2020. Effects of turbulence modulation and gravity on particle collision statistics. *Int. J. Multiph. Flow* 129:103334

Rossetti SJ, Pfeffer R. 1972. Drag reduction in dilute flowing gas-solid suspensions. *AIChE J.* 18(1):31–39

Ruiz J, Macías D, Peters F. 2004. Turbulence increases the average settling velocity of phytoplankton cells. *PNAS* 101(51):17720–24

Sabban L, van Hout R. 2011. Measurements of pollen grain dispersal in still air and stationary, near homogeneous, isotropic turbulence. *J. Aerosol Sci.* 42(12):867–82

Saito I, Watanabe T, Gotoh T. 2019. A new time scale for turbulence modulation by particles. *J. Fluid Mech.* 880:R6

Sapsis TP, Ouellette NT, Gollub JP, Haller G. 2011. Neutrally buoyant particle dynamics in fluid flows: comparison of experiments with Lagrangian stochastic models. *Phys. Fluids* 23(9):093304

Sardina G, Schlatter P, Brandt L, Picano F, Casciola CM. 2012. Wall accumulation and spatial localization in particle-laden wall flows. *J. Fluid Mech.* 699(1):50–78

Saw EW, Bewley GP, Bodenschatz E, Sankar Ray S, Bec J. 2014. Extreme fluctuations of the relative velocities between droplets in turbulent airflow. *Phys. Fluids* 26(11):111702

Saw EW, Shaw RA, Ayyalasomayajula S, Chuang PY, Gylfason A. 2008. Inertial clustering of particles in high-Reynolds-number turbulence. *Phys. Rev. Lett.* 100(21):214501

Schanz D, Gesemann S, Schröder A. 2016. Shake-The-Box: Lagrangian particle tracking at high particle image densities. *Exp. Fluids* 57(5):70

Schiller L, Naumann A. 1933. Fundamental calculations in gravitational processing. *Z. Ver. Dtsch. Ing.* 77:318–20

Schneiders L, Günther C, Meinke M, Schröder W. 2016. An efficient conservative cut-cell method for rigid bodies interacting with viscous compressible flows. *J. Comput. Phys.* 311:62–86

Schneiders L, Hartmann D, Meinke M, Schröder W. 2013. An accurate moving boundary formulation in cut-cell methods. *J. Comput. Phys.* 235:786–809

Schneiders L, Meinke M, Schröder W. 2017. Direct particle-fluid simulation of Kolmogorov-length-scale size particles in decaying isotropic turbulence. *J. Fluid Mech.* 819:188–227

Shao X, Wu T, Yu Z. 2012. Fully resolved numerical simulation of particle-laden turbulent flow in a horizontal channel at a low Reynolds number. *J. Fluid Mech.* 693:319–44

Shaw RA. 2003. Particle-turbulence interactions in atmospheric clouds. *Annu. Rev. Fluid Mech.* 35(1):183–227

Shokri R, Ghaemi S, Nobes D, Sanders R. 2017. Investigation of particle-laden turbulent pipe flow at high-Reynolds-number using particle image/tracking velocimetry (PIV/PTV). *Int. J. Multiph. Flow* 89:136–49

Smits AJ, McKeon BJ, Marusic I. 2011. High–Reynolds number wall turbulence. *Annu. Rev. Fluid Mech.* 43:353–75

Stickel JJ, Powell RL. 2005. Fluid mechanics and rheology of dense suspensions. *Annu. Rev. Fluid Mech.* 37:129–49

Sumbekova S, Cartellier A, Aliseda A, Bourgoin M. 2017. Preferential concentration of inertial sub-Kolmogorov particles: the roles of mass loading of particles, Stokes numbers, and Reynolds numbers. *Phys. Rev. Fluids* 2(2):024302

Tanaka M. 2017. Effect of gravity on the development of homogeneous shear turbulence laden with finite-size particles. *J. Turbul.* 18(12):1144–79

Tanaka M, Teramoto D. 2015. Modulation of homogeneous shear turbulence laden with finite-size particles. *J. Turbul.* 16(10):979–1010

Tanaka T, Eaton JK. 2010. Sub-Kolmogorov resolution partical image velocimetry measurements of particle-laden forced turbulence. *J. Fluid Mech.* 643:177–206

Ten Cate A, Derksen JJ, Portela LM, Van Den Akker HE. 2004. Fully resolved simulations of colliding monodisperse spheres in forced isotropic turbulence. *J. Fluid Mech.* 519:233–71

Tenneti S, Subramaniam S. 2014. Particle-resolved direct numerical simulation for gas-solid flow model development. *Annu. Rev. Fluid Mech.* 46:199–230

Tom J, Bragg AD. 2019. Multiscale preferential sweeping of particles settling in turbulence. *J. Fluid Mech.* 871:244–70

Toschi F, Bodenschatz E. 2009. Lagrangian properties of particles in turbulence. *Annu. Rev. Fluid Mech.* 41:375–404

Uhlmann M, Chouippe A. 2017. Clustering and preferential concentration of finite-size particles in forced homogeneous-isotropic turbulence. *J. Fluid Mech.* 812:991–1023

Uhlmann M, Doychev T. 2014. Sedimentation of a dilute suspension of rigid spheres at intermediate Galileo numbers: the effect of clustering upon the particle motion. *J. Fluid Mech.* 752:310–48

van Hout R. 2013. Spatially and temporally resolved measurements of bead resuspension and saltation in a turbulent water channel flow. *J. Fluid Mech.* 715:389–423

Volk R, Calzavarini E, Leveque E, Pinton JF. 2011. Dynamics of inertial particles in a turbulent von Kármán flow. *J. Fluid Mech.* 668:223–35

Voth GA, La Porta A, Crawford AM, Alexander J, Bodenschatz E. 2002. Measurement of particle accelerations in fully developed turbulence. *J. Fluid Mech.* 469:121–60

Voth GA, Soldati A. 2017. Anisotropic particles in turbulence. *Annu. Rev. Fluid Mech.* 49:249–76

Vreman A. 2017. A staggered overset grid method for resolved simulation of incompressible flow around moving spheres. *J. Comput. Phys.* 333:269–96

Wan ZY, Sapsis TP. 2018. Machine learning the kinematics of spherical particles in fluid flows. *J. Fluid Mech.* 857:R2

Wang G, Abbas M, Climent E. 2018. Modulation of the regeneration cycle by neutrally buoyant finite-size particles. *J. Fluid Mech.* 852:257–82

Wang G, Fong KO, Coletti F, Capecelatro J, Richter DH. 2019. Inertial particle velocity and distribution in vertical turbulent channel flow: a numerical and experimental comparison. *Int. J. Multiph. Flow* 120:103105

Wang LP, Maxey MR. 1993. Settling velocity and concentration distribution of heavy particles in homogeneous isotropic turbulence. *J. Fluid Mech.* 256:27–68

Wang LP, Stock DE. 1993. Dispersion of heavy particles by turbulent motion. *J. Atmos. Sci.* 50(13):1897–913

Wang Y, Sierakowski A, Prosperetti A. 2019. Rotational dynamics of a particle in a turbulent stream. *Phys. Rev. Fluids* 4(6):064304

Wilkinson M, Mehlig B. 2005. Caustics in turbulent aerosols. *EPL* 71(2):186

Willen DP, Prosperetti A. 2019. Resolved simulations of sedimenting suspensions of spheres. *Phys. Rev. Fluids* 4(1):014304

Yang T, Shy S. 2005. Two-way interaction between solid particles and homogeneous air turbulence: particle settling rate and turbulence modification measurements. *J. Fluid Mech.* 526:171–216

Yavuz M, Kunnen R, Van Heijst G, Clercx H. 2018. Extreme small-scale clustering of droplets in turbulence driven by hydrodynamic interactions. *Phys. Rev. Lett.* 120(24):244504

Yeo K, Dong S, Climent E, Maxey MR. 2010. Modulation of homogeneous turbulence seeded with finite size bubbles or particles. *Int. J. Multiph. Flow* 36(3):221–33

Yeo K, Maxey MR. 2010. Dynamics of concentrated suspensions of non-colloidal particles in Couette flow. *J. Fluid Mech.* 649:205–31

Yousefi A, Ardekani MN, Brandt L. 2020. Modulation of turbulence by finite-size particles in statistically steady-state homogeneous shear turbulence. *J. Fluid Mech.* 899:A19

Yousefi A, Ardekani MN, Picano F, Brandt L. 2021. Regimes of heat transfer in finite-size particle suspensions. *Int. J. Heat Mass Transf.* 177:121514

Yudine M. 1959. Physical considerations on heavy-particle diffusion. *Adv. Geophys.* 6:185–91

Zade S. 2019. *Experimental studies of large particles in Newtonian and non-Newtonian fluids*. PhD Thesis, KTH R. Inst. Technol., Stockh., Swed.

Zade S, Costa P, Fornari W, Lundell F, Brandt L. 2018. Experimental investigation of turbulent suspensions of spherical particles in a square duct. *J. Fluid Mech.* 857:748–83

Zade S, Fornari W, Lundell F, Brandt L. 2019. Buoyant finite-size particles in turbulent duct flow. *Phys. Rev. Fluids* 4(2):024303

Zaidi AA, Tsuji T, Tanaka T. 2014. Direct numerical simulation of finite sized particles settling for high Reynolds number and dilute suspension. *Int. J. Heat Fluid Flow* 50:330–41

Zamansky R, Coletti F, Massot M, Mani A. 2014. Radiation induces turbulence in particle-laden fluids. *Phys. Fluids* 26(7):071701

Zamansky R, Coletti F, Massot M, Mani A. 2016. Turbulent thermal convection driven by heated inertial particles. *J. Fluid Mech.* 809:390–437

Zhang Q, Prosperetti A. 2010. Physics-based analysis of the hydrodynamic stress in a fluid-particle system. *Phys. Fluids* 22(3):033306

Zhao L, Andersson HI, Gillissen J. 2010. Turbulence modulation and drag reduction by spherical particles. *Phys. Fluids* 22(8):081702

Contents

Indexes

Errata

An online log of corrections to *Annual Review of Fluid Mechanics* articles may be found
at http://www.annualreviews.org/errata/fluid